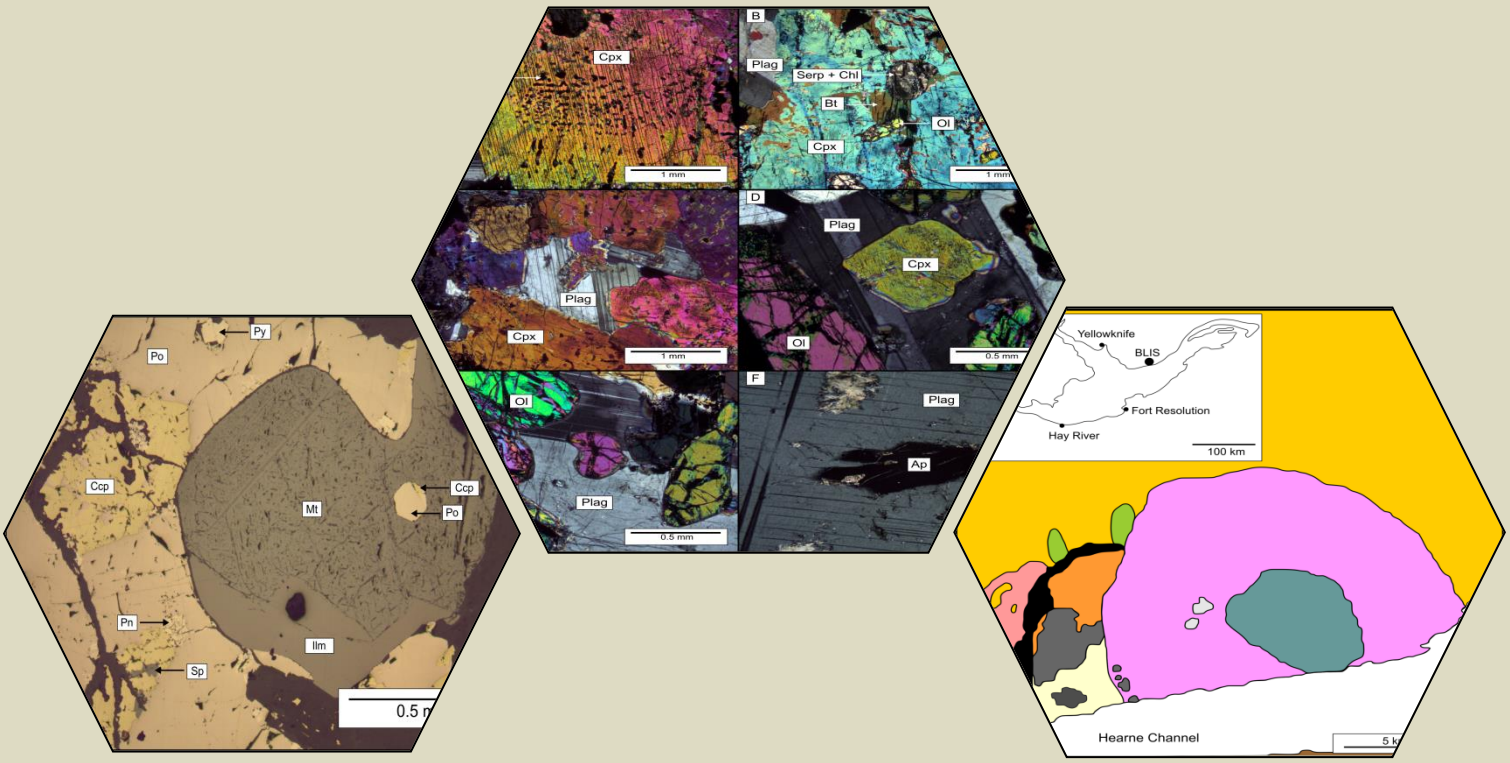

NWT Open File 2014-08

Mineralogy, geochemistry, stable isotopes, and preliminary fluid inclusion analysis of the Caribou Lake mafic-ultramafic intrusion, Northwest Territories, Canada

K. Neyedley, J. Hanley, H. Falck, M. Fayek, R. Sharpe

*Recommended Citation**: Neyedley, K., Hanley, J., Falck, H., Fayek, M. and Sharpe, R, 2014.** *Mineralogy, geochemistry, stable isotopes, and preliminary fluid inclusion analysis of the Caribou Lake mafic-ultramafic intrusion, Northwest Territories, Canada. Northwest Territories Geoscience Office Open File 2014-08.*

Northwest Territories

NORTHWEST TERRITORIES GEOSCIENCE OFFICE
PO Box 1320, 4601-B 52 Avenue, Yellowknife, NT X1A 2L9

Northwest Territories Geoscience Office
Open File 2014-08

Mineralogy, geochemistry, stable isotopes, and preliminary fluid inclusion analysis of the Caribou Lake mafic-ultramafic intrusion, Northwest Territories, Canada

K. Neyedley[1], J. Hanley[1], H. Falck[2], M. Fayek[3], R. Sharpe[3]

[1]Department of Geology
Saint Mary's University
923 Robie Street
Halifax, NS
B3H 3C3

[2]Northwest Territories Geoscience Office
PO Box 1320
4601-B 52 Avenue
Yellowknife, NT
X1A 2L9

[3]Department of Geological Sciences
University of Manitoba
125 Dysart Road
Winnipeg, MB
R3T 2N2

Introduction

The mafic-ultramafic Caribou Lake Intrusion (CLI), located roughly 90 km southeast of Yellowknife in the Northwest Territories, contains minor Ni-Cu-platinum group element (PGE) mineralization hosted mainly in rock units of gabbroic composition. Mineralization consists of massive to disseminated pyrrhotite with lesser amounts of chalcopyrite, pentlandite, pyrite, and sphalerite. No PGE mineral grains have been found to date, but assay results from a fine-grained gabbro with trace amounts of sulfides indicate 214 ppm Pt+Pd (Marmont, 2007). A major aspect of this project is to characterize the mineralization and its associated host rocks. Detailed core logging and sampling of a drill hole containing highly disseminated sulfide over ~10m was conducted over the summer of 2013 and two other drill holes were logged and sampled in order to examine the internal stratigraphy of the intrusion. Additional samples of massive sulfide mineralization and their associated host rocks were also collected from drill holes. Geochemical analyses of the intrusion reveal that it is tholeiitic in composition and alteration has not significantly changed the overall geochemistry of the rocks. Fluid inclusions in apatite and quartz are well preserved in various coarse grained gabbroic units and will be studied in this project.

A major question to be answered by this study is have fluids remobilized metals in the system and therefore decreased the tenor of sulfide mineralization? Whole rock geochemical results have shown that some units can be extremely enriched in vanadium (up to 2.3 wt%). Magnetite has up to 1.3 wt% vanadium and can display two styles of ilmenite exsolution: blebby texture, where ilmenite and magnetite occur as a composite grain with a grain of ilmenite on the edge of magnetite and trellis pattern exsolution, where ilmenite exsolves from titanomagnetite along the {111} plane to produce a crosshatched exsolution pattern. Questions that have arisen from the observations of high abundances of Fe-Ti oxides in the intrusion include: What was the fO_2 conditions of the intrusion, which can be constrained by reconstructing the composition of the original titanomagnetite, and is there enough magnetite with appreciable vanadium concentrations to validate further exploration in the area.

Regional Geology

The Caribou Lake mafic-ultramafic intrusion is located approximately 90km southeast of Yellowknife, Northwest Territories along the Hearne Channel, Great Slave Lake and lies at the southern margin in the Slave Province of the Canadian Shield (Figure 1 and Figure 2). The CLI comprises the western suite of the alkaline to peralkaline Blatchford Lake Intrusive Suite (BLIS), which is thought to be related to the formation of the Authapuscow Aulacogen and the associated failed rift (Bowring et al, 1984; Hoffman, 1980) that could have promoted crustal thinning, decompressional melting and served as a conduit for mantle derived magmas (Mumford, 2013). The BLIS intrudes sedimentary rocks of the Archean Yellowknife supergroup, Morose granite, and the Defeat granodiorite (Davidson, 1972, 1978). A geophysical gravity study by Birkett et al (1994) and Pilkington (2012) suggested that the BLIS is a relatively thin tabular body, approximately 1km thick with deep mafic (CLG) roots at the western contacts. The CLG also appears to extend under the Grace Lake granite for almost half of the entire complex.

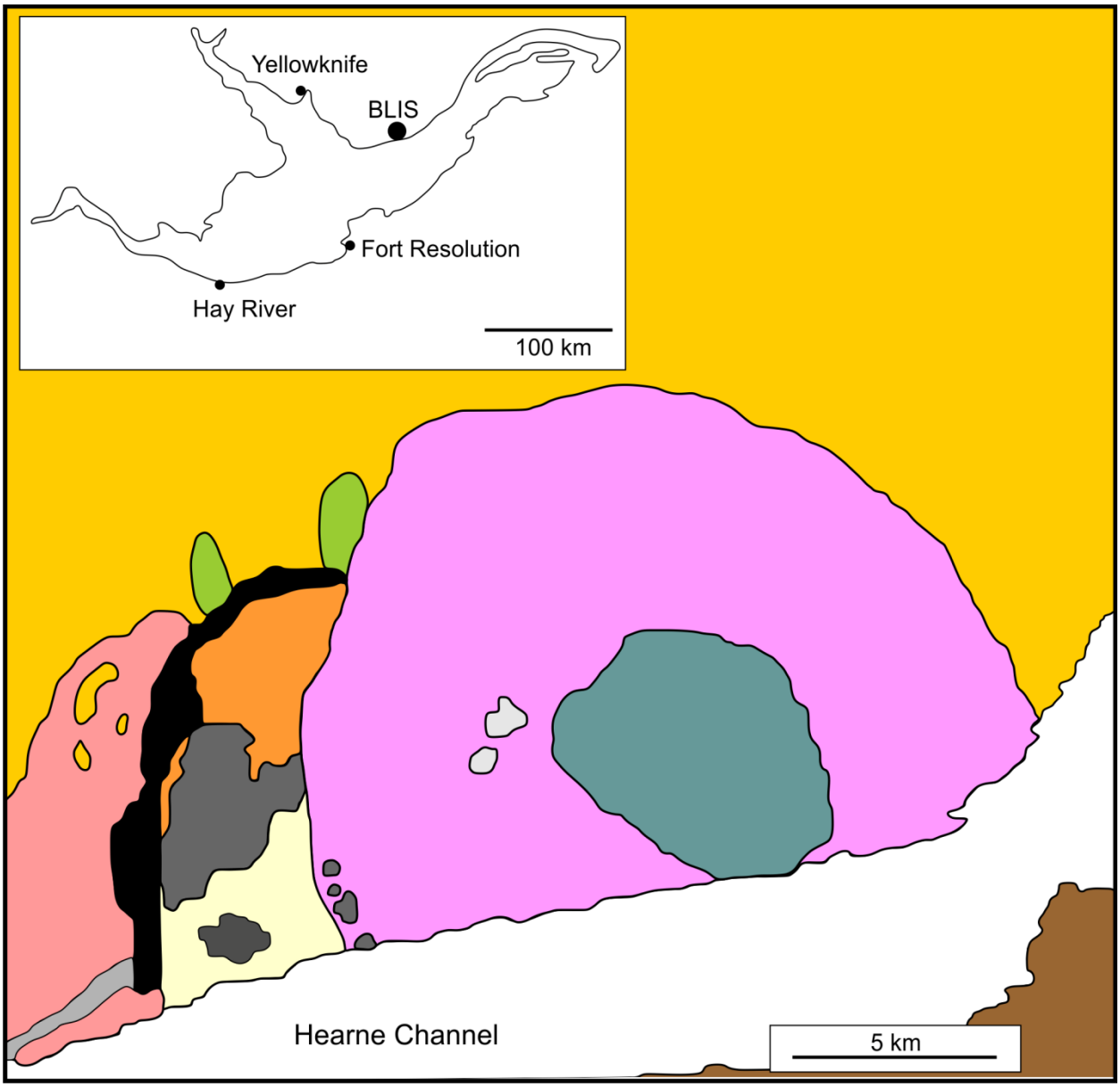

Figure 1: *Simplified geology of the Blatchford Lake intrusive suite, modified after Davidson (1982) and Mumford (2013).*

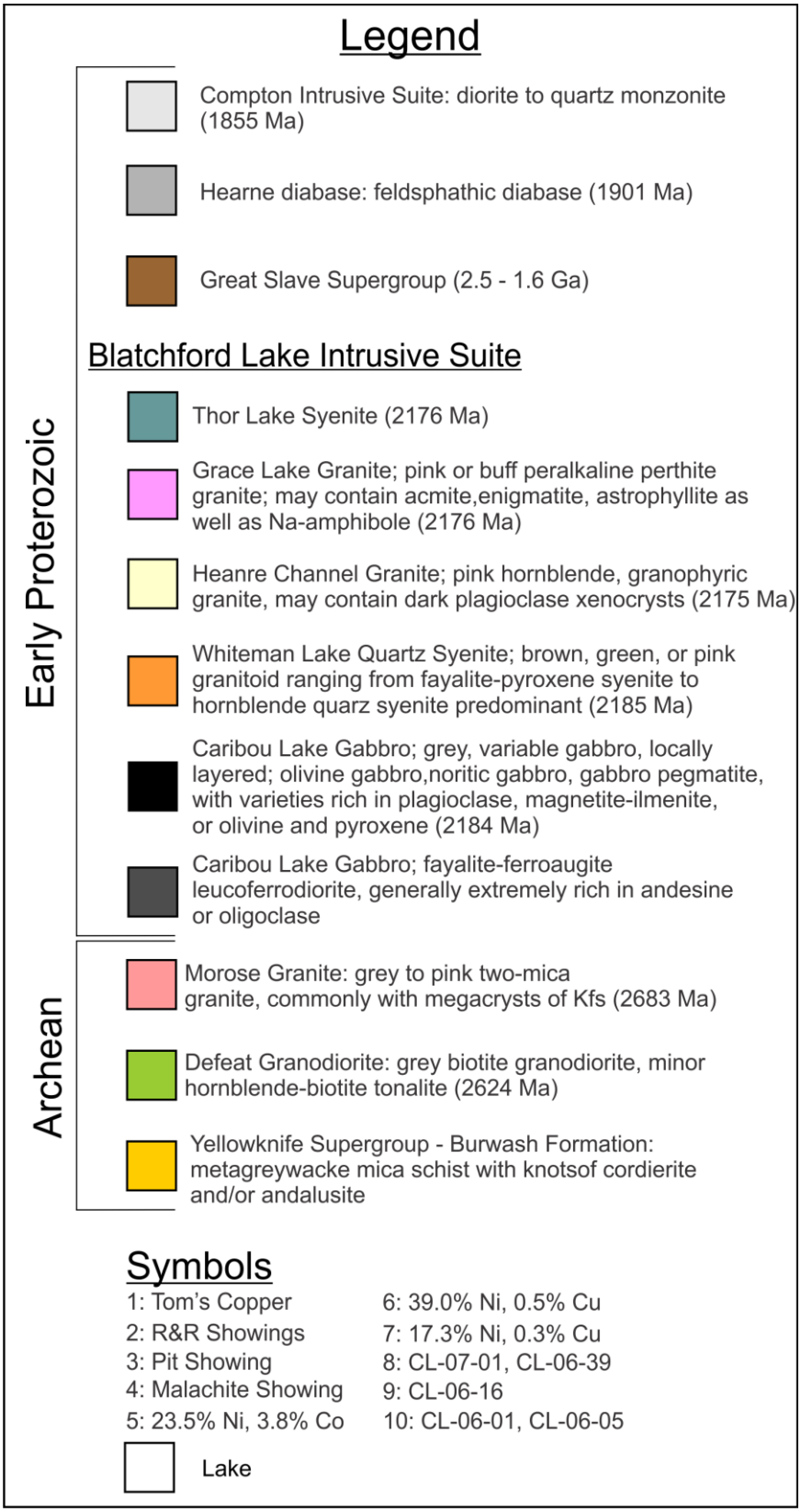

Figure 2: *Geology legend for Figure 1 and Figure 3.*

The first detailed mapping of the BLIS was undertaken by Davidson (1972). His subsequent work (Davidson, 1978, 1981, 1982) identified six distinct units based on field relationships and geochronology:

1) Caribou Lake gabbro ranging to leucoferrodiorite (2184 ± 2 Ma, Mumford, 2013),
2) Whiteman Lake quartz syenite (2185 ± 2 Ma, Bowring et al, 1984),
3) Hearne Channel granite (2175 ± 5 Ma, Bowring et al, 1984),
4) Mad Lake granite (2166 ± 47 Ma, Wanless et al, 1979),
5) Grace Lake granite (2176.2 ± 1.3 Ma, Sinclair et al, 1994),
6) Thor Lake syenite (2164 ± 11 Ma, Mumford, 2013).

Based on geochemistry (Davidson, 1981), the BLIS could be broken into two distinct portions; an older sub-alkaline western lobe (Units 1-4) and a younger peralkaline eastern lobe (Units 5-6). Mumford (2013) has described units 2 to 4 as coeval multi-phase intrusives, (based on contacts and variations within the granitic intrusions), that show large scale changes from north to south; therefore, these units (2, 3, 4) are transitional and the Mad Lake granite can be distributed between the northern Whiteman Lake and southern Hearne Channel, eliminating the Mad Lake granite from the intrusive suite.

Exploration History

The Earl Jack Syndicate investigated aeromagnetic anomalies during 1963 in the Caribou Lake area. They discovered Fe-Ti occurrences with up to 15% oxide corresponding to aeromagnetic highs within an anorthositic gabbro in the higher grade zones, assays returned values of 30% Fe and 10% TiO_2. No claims were staked because zones of titanium and iron mineralization were deemed too small to be considered economic at the time (Curry et al, 1963). Shield Resources performed magnetic surveys during the 1960's and discovered sulfide occurrences associated with magnetic lows. Numerous trenches were also blasted during the time Shield held claims in the area, several of which contained niccolite hosted in carbonate veins (Curry, 1969).

Airborne magnetic and EM survey were conducted by New Caledonia Mining in 1994, also collected till samples looking for diamond indicator minerals. A few magnetic anomalies were identified, with a follow-up ground magnetic survey suggested for one of them. They also suggested that there were no significant concentrations of base metals occurring in the gabbroic units (Warman and Gelo, 1995).

In 2004 Kodiak Exploration performed reconnaissance prospecting of the Caribou Lake gabbro. They sampled previously known niccolite showings and one sample returned assay values of 38.2% Ni and 3.8% Co. One sample of gabbro within the Whiteman Lake syenite was collected and had values of 19.7% Cu and 0.3% Ni. A total of 130 samples were sent for assay analysis (Marmont, 2006). During the summer of 2005 Kodiak Exploration hired Aurora Geoscience to perform a prospecting and sampling program as well as to investigate the areas around the magnetic anomalies discovered by New Caledonia Mining. Aurora Geosciences' program resulted in 714 samples submitted for assay. Of all the 2004 and 2005 samples submitted for assay (n=844), 91 came back with values greater than 0.1% Cu and 41 with greater

than 0.1% Ni. Because of the results produced during the sampling program, an airborne VTEM electromagnetic and magnetic survey over the Caribou Lake intrusion was conducted. From these surveys thirteen strong EM anomalies were identified and twelve of them occurred in the mafic-ultramafic units of the Caribou Lake intrusion (Marmont, 2006).

Kodiak's prospecting work continued into 2006 and focused on areas located around the anomalies from the EM and magnetic surveys. This program identified new anomalies that contain modest amounts of PGE (30 ppb Pt-Pd) and one sample with Pt and Pd values of 97 and 25 ppb Pd respectively. Some mineralized carbonate veins were also found during this program, which returned assay values of 8.4% Ni and 1.25% Co (Marmont, 2006).

In 2006 Kodiak also undertook a drilling program that was designed to test the EM anomalies, explore the contact of the CLI, test the depth of surface showings, as well as to determine the stratigraphy of the CLI. The first, third and fifth drill holes produced the best results of the program, encountering massive sulfides with grades ~0.53% Ni and ~0.7% Cu (Marmont, 2006). Kodiak continued its drill program in 2007 with an additional fifteen drill holes to explore the basal contact of the CLI, re-test some VTEM anomalies and to improve their understanding of the stratigraphy. No significant sulfide intersections were encountered during the 2007 drill program (Marmont, 2007).

Study Area

The oldest part of the Blatchford Lake Intrusive Suite is the Caribou Lake gabbro (2184 ± 2 Ma, Mumford, 2013) which intrudes into the Archean sedimentary rocks of the Yellowknife Supergroup, the Morose granite, and the Defeat granodiorite (Figure 2 and Figure 3), which contain minor amounts of disseminated pyrrhotite (Davidson, 1982). Contacts between the CLI and its Archean host rocks are not commonly observed due to cover by vegetation, swamps, or lakes. Davidson (1978) described a chilled margin along the western contact and also observed progressive changes from west to east across the gabbro starting with pegmatitic patches in massive olivine gabbro along the west and north shores of Caribou and Whiteman Lakes transitioning into a massive to faintly layered noritic gabbro with plagioclase defining a weak foliation, with the most eastern portion of the gabbro identified as a leucoferrodiorite.

Drilling results in 2006 were moderately successful, with massive to heavily disseminated sulfide encountered in four drill holes approximately 3km south of Caribou Lake (Figure3), including the first hole which intersected 0.53% Ni and 0.7% Cu over 3.18m (Marmont, 2006). The other intersections of massive to highly disseminated sulfide have similar Ni and Cu grades (Marmont, 2006). Sulfides are hosted by a fine to medium grained gabbro and are primarily composed of pyrrhotite with lesser amounts of chalcopyrite and pyrite (Marmont, 2006). Drilling results in 2007 proved to be unsuccessful in the effort to find more massive sulfide intersections (Marmont, 2007).

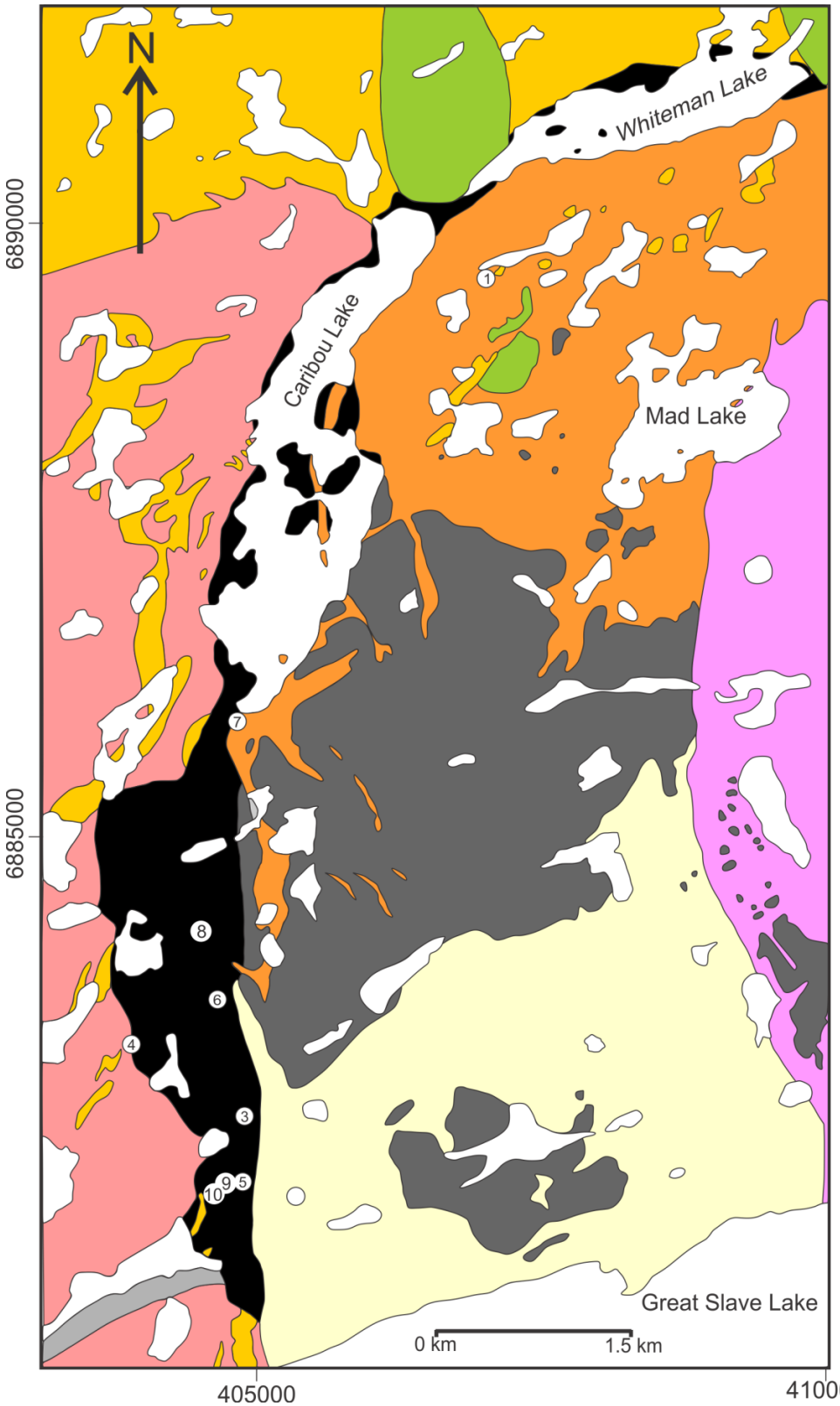

Figure 3: *Detailed geology of the western portion of the Blatchford Lake intrusive suite, modified after Davidson (1982) and Mumford (2013).*

Objectives

The overall goal of the project is to develop a model for Ni-Cu-PGE and to compare the CLI to other economic deposits in tholeiitic layered intrusions in other locales. The results of the project will provide insight into primary process of sulfide formation and secondary processes leading to alteration within the CLI and also processes affecting the metal tenor of the system. Detailed objectives of the study are:

1. The characterization of primary and alteration mineralogy and sulfides occurrences. The goals are to: i) develop a paragenesis for mineralization and primary silicate minerals, ii) develop a stratigraphy for the intrusion to understand how many different magmatic pulses were involved in the development of the system, iii) document the relationships between the sulfide and silicate minerals as well as the effect of alteration on the distribution of sulfides, and iv) identify where PGE and other accessory metals occur (such as As, Te, Bi, Au, Ag), whether in discrete PGMs or within base metal sulfides.

2. The characterization of whole rock and trace element geochemistry of mineralized and host rock lithologies within the CLI. The geochemistry of the CLI will be compared to other mafic-ultramafic intrusions globally. The role of alteration and fluid interaction on primary sulfide mineralogy will be assessed by comparing altered and unaltered units.

3. A study of fluid and melt inclusions (microthermometry and trace element compositions). The goals are to: i) identify all fluid inclusions types (i.e. vapor-rich, vapor-poor, halite bearing, aqueous, etc.) ii) constrain the temperature and depth of emplacement of various stages of the intrusion using FI microthermometry, should inclusions be primary in origin, iii) determine what types of fluids (magmatic, metamorphic, meteoric) were involved in metal remobilization and alteration of the system, and iv) measure trace element composition of inclusions through Laser Ablation Inductively Couple Plasma Mass Spectrometry (LA-ICPMS) to determine if any metals have been remobilized in fluid inclusions present in the system and to determine the metal contents in sulfide and silicate melt inclusions that are free of alteration.

4. Characterize sulfur isotopes by bulk and *in situ* analysis. Sulfur isotopes can be an indicator of country rock assimilation, which has been shown to be an important factor in formation of magmatic Ni-Cu-PGE sulfide deposits. In situ analysis by secondary ion mass spectrometry (SIMS) will allow for different generations and styles of sulfide mineralization to be analyzed.

Methodology

During the winter of 2013 a total of 29 samples were collected from Kodiak Explorations 2007 drill program by Hendrik Falck for the purpose of preliminary petrography of various units within the CLI (refer to Appendix A for sample list). During the summer of 2013, an additional 266 sample were collected from numerous drill holes from the 2006 and 2007 drill programs. Of the 266 collected only 112 were sent to Vancouver Petrographics and the Ontario Geological Survey Geolabs for whole rock and trace element analysis as well as 20 samples for Ni-sulfide fire assay for PGE contents (refer to Appendix B for sample list).

The majority of samples were collected from only three drill holes that were also descriptively logged; 1) CL-06-16 (170.7 m), 2) CL-06-39 (163.05 m), and 3) Cl-07-01(481.4 m). A total of 28 samples were sent for analysis from drill hole CL-06-16, nine of which were within a 10 m interval of heavily disseminated sulfide, the other samples represented lithology changes throughout the length of the hole. In CL-06-39, a thick ultramafic succession of approximately 50m had been intersected and represented the thickest ultramafic package encountered in drilling; a total 29 samples were shipped for analysis representing lithology changes. CL-07-01 and CL-06-39, which were drilled 200 m apart, were logged to correlate units between the two drill holes. Thirty nine samples were sent for analysis from CL-07-01, representing lithology changes throughout the length of the hole. The remaining 16 samples sent for analysis came from various drill holes representing other styles of mineralization (i.e. semi-massive to massive), host rock lithologies, and other units composing the BLIS.

The petrographic characteristics of thin sections were determined using a Nikon Eclipse H550L microscope, which has the capability to use transmitted and reflected light. The characterization of base metal sulfides and discrete mineral phases has been conducted using a LEO1450VP scanning electron microscope (SEM) at Saint Mary's University, equipped with an energy dispersive X-ray (EDS) Oxford INCA 80mm^2 silicon drift detector (SDD) capable of quantitative analysis. Measurements of all analysis were conducted at a working distance of ~20mm, with a beam current of 40uA and accelerating voltage of 25.00-30.00 kV.

Core samples were sent to the Ontario Geological Survey GeoLabs in Sudbury, Ontario for whole rock and trace element geochemistry which were determined by X-ray fluorescence spectrometry (XRF) and inductively-coupled plasma mass spectrometry (ICP-MS). Samples that contained large enough sulfides to be drilled with a ~2 mm drill bit, were sampled and sent to the Queens University Stable Isotope lab for analysis by stable isotope ratio mass spectrometer (IRMS).

Sulfur isotope compositions of primary and secondary pyrrhotite were determined *in situ* using a CAMECA IMS 7f secondary ion mass spectrometer (SIMS) at the University of Manitoba. A cesium (Cs^+) primary beam with a 2 nA current, was accelerated (+10 kV) onto the sample surface with a sputtering diameter of 15 μm; the instrument operated at a 200 V sample offset, -9 kV secondary accelerating voltage and at mass resolving power of 347.

During the measurement process by SIMS, an intrinsic mass dependent bias is introduced, which is referred to as instrumental mass fractionation (IMF) and typically favours the low mass isotope. The greatest contributor to the IMF is the ionization process, which depends most strongly upon sample characteristics (i.e., chemical composition). This is referred to as compositionally dependent fractionation or "matrix effects" (e.g., Riciputi *et al.* 1998). Therefore, accurate isotopic SIMS analysis requires that IMF be corrected for by standardizing the IMF using mineral standards that are compositionally similar to the unknown. SIMS results from the standard are compared to its accepted isotopic composition in order to calculate a correction factor that is applied to the unknowns measured during the same analysis session (e.g., Holliger and Cathelineau, 1988).

A grain of Anderson pyrrhotite with a $\delta^{34}S$ value of 1.4±0.3‰ from the Anderson Lake Mine, Manitoba, Canada was used as the sulfur isotope standard (Crowe and Vaughn, 1996). Spot-to-spot reproducibility for Anderson pyrrhotite was 0.3 and precision for individual analysis was 0.3 for $\delta^{34}S$ values. Therefore, 2σ errors for oxygen and sulfur isotope analysis are 0.3.

Isotopic data are reported in standard δ-notation relative to the appropriate standard, Canyon Diablo Troilite (CDT) for $^{34}S/^{32}S$. The equation for calculating δ values in units of per mil (‰) is:

$$\delta_{sample} = (R_{sample}/R_{std}-1)x10^3 \quad [1]$$

where R_{sample} and R_{std} are the absolute isotope ratios in sample and standard, respectively. Isotope ratios measured by SIMS were compared to the accepted ratios (calculated from δ values determined by conventional analyses and gas source mass spectrometry) for each mineral using equation [2]:

$$R_{sample}=[(\delta_{sample}/10^3)+1]R_{std} \quad [2]$$

where R_{std} ($^{34}S/^{32}S$) for CDT is 4.450045 x 10^{-2} (Jenson & Nakai, 1962). These data can be used to calculate isotope mass fractionation that occurs during SIMS analysis by using equation [3]:

$$\alpha SIMS=R_{SIMS}/R_{conv.} \quad [3]$$

where R_{SIMS} is the ratio measured by SIMS and R_{conv} is the accepted ratio measured by conventional gas source mass spectrometry. These ratios can be converted to ‰ notation by:

$$\delta_{bias}= [(R_{SIMS}/R_{conv.})-1] \times 10^3 \quad [4]$$

Results

Drill Hole CL-06-16

Drill hole CL-06-16 is a 170.6m long vertical drill hole that was drilled into the southern portion of the CLI (Figure 3). This hole was chosen for the study based on its highly disseminated sulfide mineralization. The hole is predominately composed of a gabbroic unit that varies from fine to coarse grained. Plagioclase and clinopyroxene modal proportions are relatively consistent throughout the unit, ranging from 30-50% plagioclase and 20-35% clinopyroxene. Orthopyroxene and olivine vary significantly through the gabbroic unit, ranging from 0-10% for both minerals. Alteration intensity varies throughout the gabbro as well. Short intervals of a melagabbro were observed at 34.7-36.1m in the core, which will be referred to as a clinopyroxenite. The upper and lower contacts with the surrounding gabbro are gradational. Clinopyroxenite consists of 5-10% plagioclase, 50-75% clinopyroxene, 0-15% olivine, Fe-Ti oxides 10-15%, and 3-5% pyrrhotite with trace chalcopyrite. From 51.8 m to 64.5 m, moderate to heavily disseminated sulfides occur, primarily pyrrhotite with minor amounts of chalcopyrite. A small anorthosite unit occurs at 90 metres depth within the gabbro and is only ~10 cm in length. From 87.5-88.1 m and 92.2-108.9 m alteration zones contain abundant calcite-quartz veinlets and stringers consisting of epidote, pyrite, serpentine and chlorite. Minor amounts of bleaching are present within the zone as well as minor amounts of hematite alteration. Below the alteration zone is a thick interval of quartz syenite (108.9-139.05 m) and then a plagioclase rich diabase

(139.05-151.5 m). A small interval of gabbro occurs from 151.5-153.3 m. The hole ends in plagioclase rich diabase. Stratigraphic column showing variations in mineralogy and alteration is illustrated in Figures 4, 5 and 6.

Drill Hole CL-06-39

Drill hole CL-06-39 is a 163.1m long vertical drill hole that was drilled approximately 2000 m north of CL-06-16 (Figure 3). The significance of this hole is that it contains a ~70 m thick interval of ultramafic, the thickest ultramafic succession identified by Kodiak's drill program. The upper ~27 m of the hole is mainly composed of a gabbro with grain sizes varying from medium to coarse grained and relatively consistent modal proportions of plagioclase (45-50%), clinopyroxene (40-45%,) and Fe-Ti oxides (2-7%). A few pegmatitic gabbros were also encountered within the first 27m, one at 4.1 m and the other at 6.85 m. These pegmatites are different from the host gabbro in modal mineral abundances, with the pegmatite at 4.1m being composed of primarily of clinopyroxene (~65%) and plagioclase (~35%) and the pegmatite at 6.9m being composed of primarily of plagioclase (~65%) and clinopyroxene (30%). A small 60cm interval of dunite occurs at 20.3m within the gabbro and is strongly altered. The gabbros upper contact with the dunite is slightly chilled for 2cm downhole, where grain sizes change from <1mm at the contact to 2-8mm after the contact. A thick ultramafic interval was encountered from 27.7m to 97.45m and is primarily composed of olivine (60-90%), clinopyroxene (10-20%) and plagioclase (0-5%), varying between dunite, lherzolite and wehrlite. Rarely, plagioclase modal abundances reach ~10-15%, as such; some short intervals can be classified as troctolite (e.g. 83.9m). Iron-titanium oxides vary considerably throughout the ultramafic interval, with modal abundances ranging anywhere from trace amounts to 35% of a given interval. A short (40cm) interval of gabbro occurs within the ultramafics, with sharp contacts and abrupt changes in modal proportions, but magnetite seems to concentrate around the contacts. From 82.1-84.8m, a carbonate alteration zone is present, which occurs just before a small fault surface at 85.7m. From 97.45-118.45m is composed primarily of various types of gabbros that can be rich in plagioclase, clinopyroxene, or Fe-Ti oxides. Each type of gabbro is generally a short interval (<20cm) and contacts appear to be gradational. Rare, thin ultramafic and oxide-rich ultramafic sections are also present within this interval. Two pegmatites occur within this interval, one at 100m, which is an anorthosite and another at 103.9m, which is an olivine gabbro. A magnetite rich (~70% Fe-Ti oxides) interval also occurs at 103.7m shortly before the pegmatite. After the varied gabbro interval, a uniform gabbro occurs until 122.95m, where an anorthosite is intersected, which appears to be highly altered. The lower contact of the anorthosite is gradational with a gabbro below at 125.9m, while the top contact of the anorthosite is sharp. The gabbro from 125.9-152.9m is similar to the uniform gabbro present above the anorthosite. At 152.9m, the lithology changes into an oxide-rich dunite, with Fe-Ti oxides composing 20-35% of the interval. This oxide-rich dunite, occurs until 156.9m where a sharp contact occurs with a gabbroic pegmatite and the pegmatite is only present for 20cm before the lithology changes back into a gabbro at 157.2m. The gabbro occurs for 3m and then the unit changes into a syenite at 160.3m, which then ends the length of the drill hole at 163.05. Stratigraphic column showing variations in mineralogy and alteration is illustrated in Figures 7 and 8.

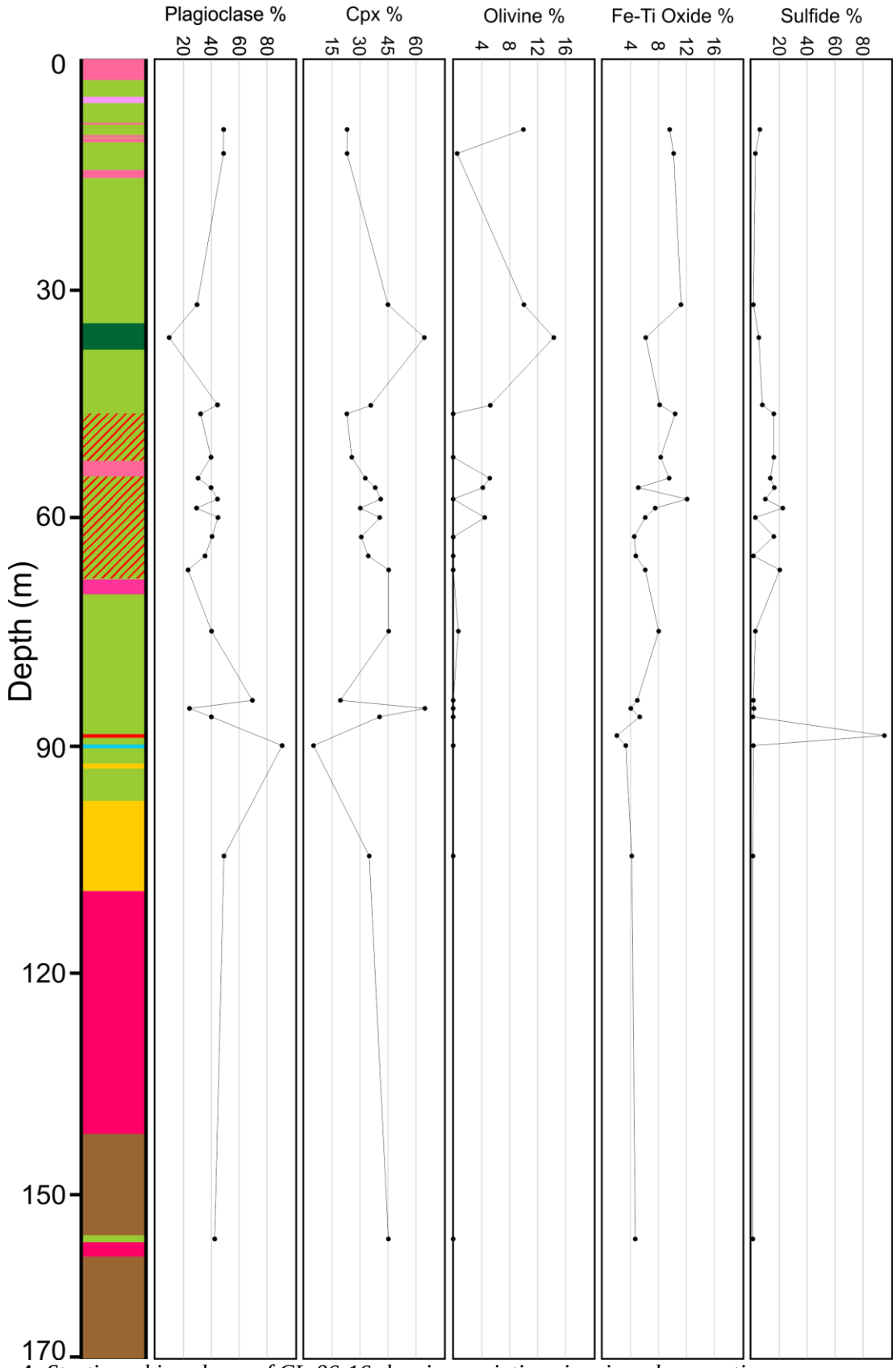

Figure 4: *Stratigraphic column of CL-06-16 showing variations in mineral proportions.*

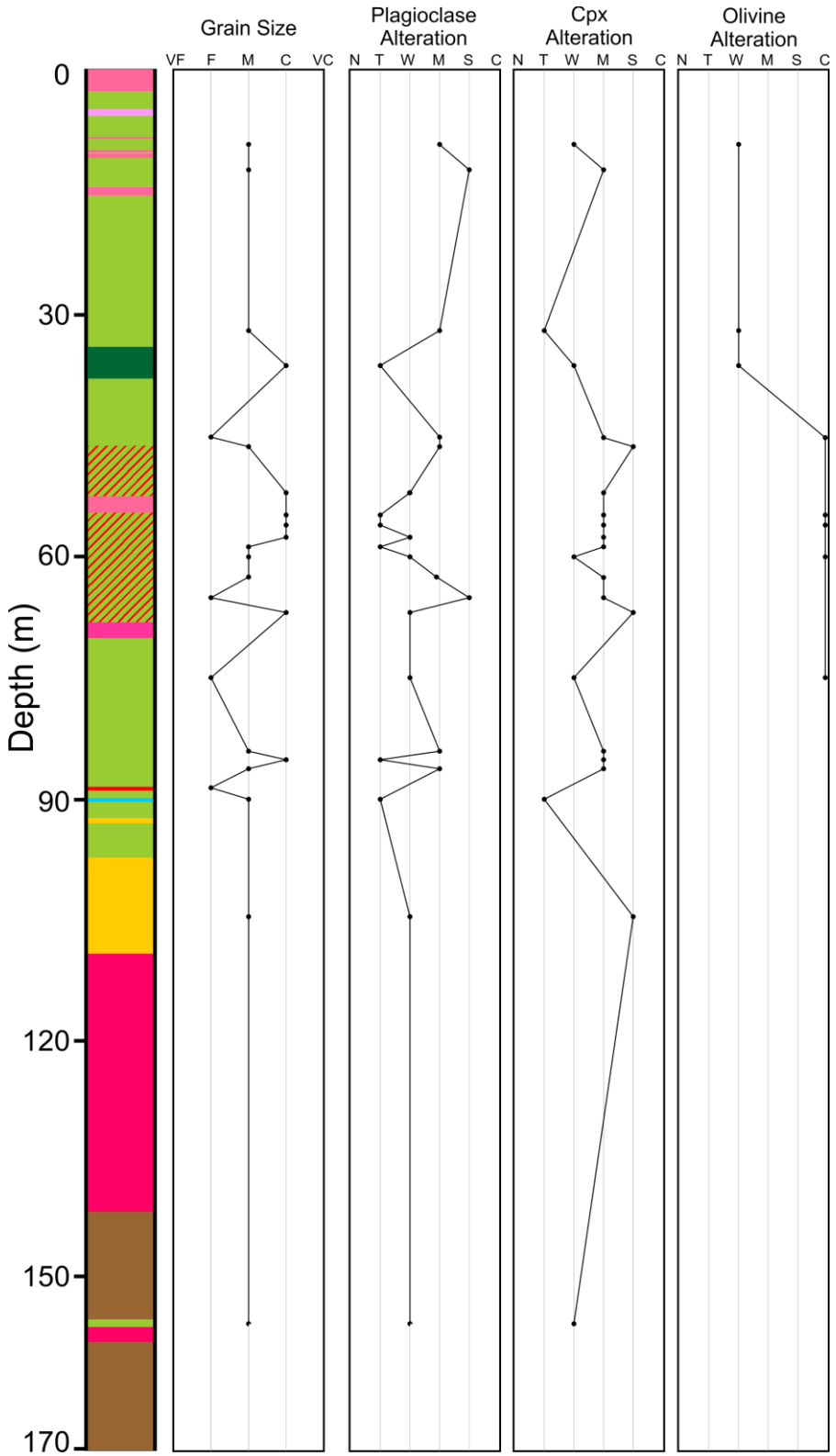

Figure 5: *Stratigraphic column of CL-06-16 showing variations in alteration. Grain sizes: Very fine (VF) = <0.8mm; Fine (F) = 0.8-1.5; Medium (M) = 1.5-3mm; Coarse (C) 3-7mm; Very coarse = 7-12mm.*

Figure 6: *Legend for stratigraphic columns in Figures 4, 5, 7 and, 8.*

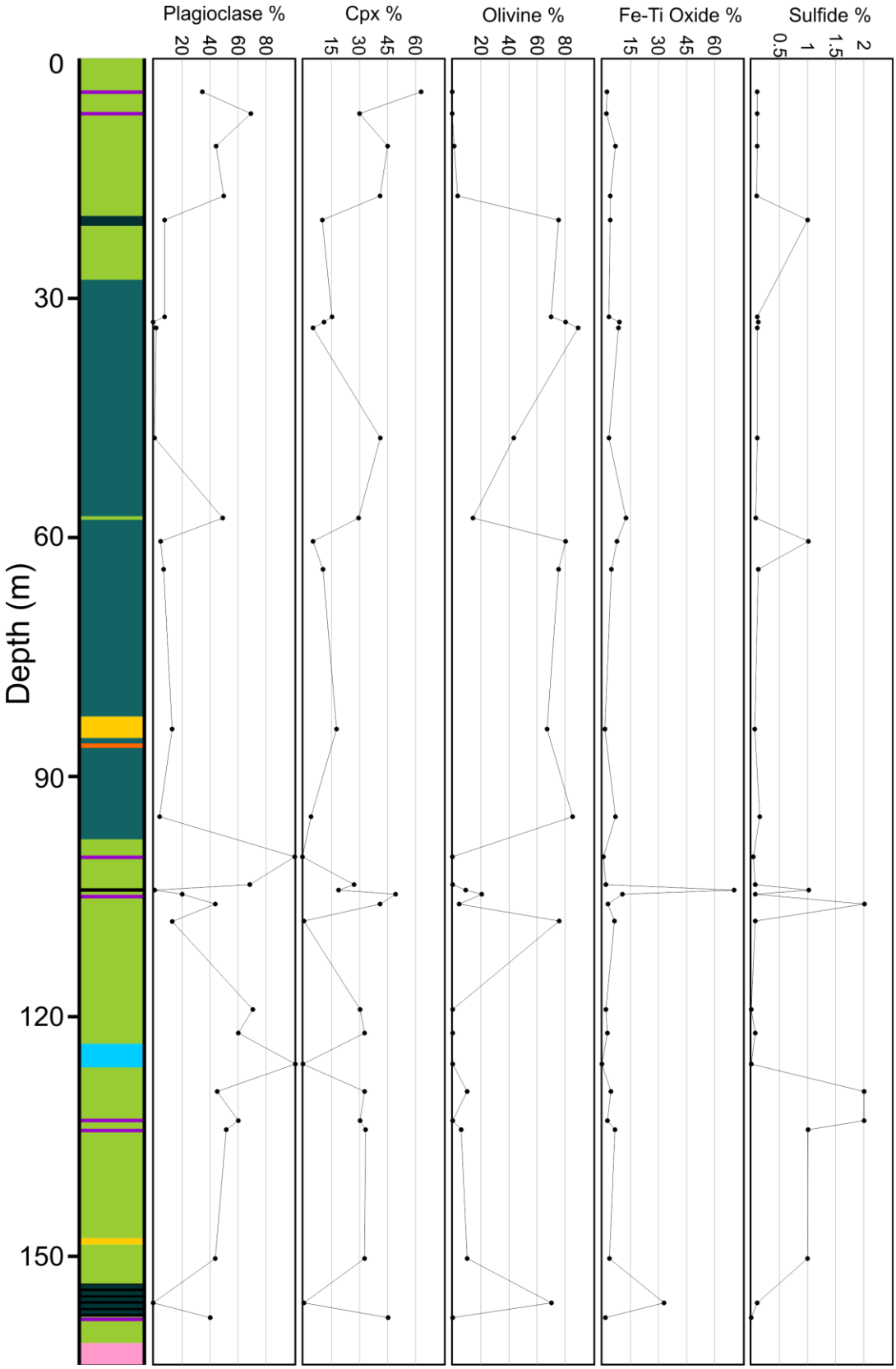

Figure 7: *Stratigraphic column of CL-06-39 showing variations in mineral proportions.*

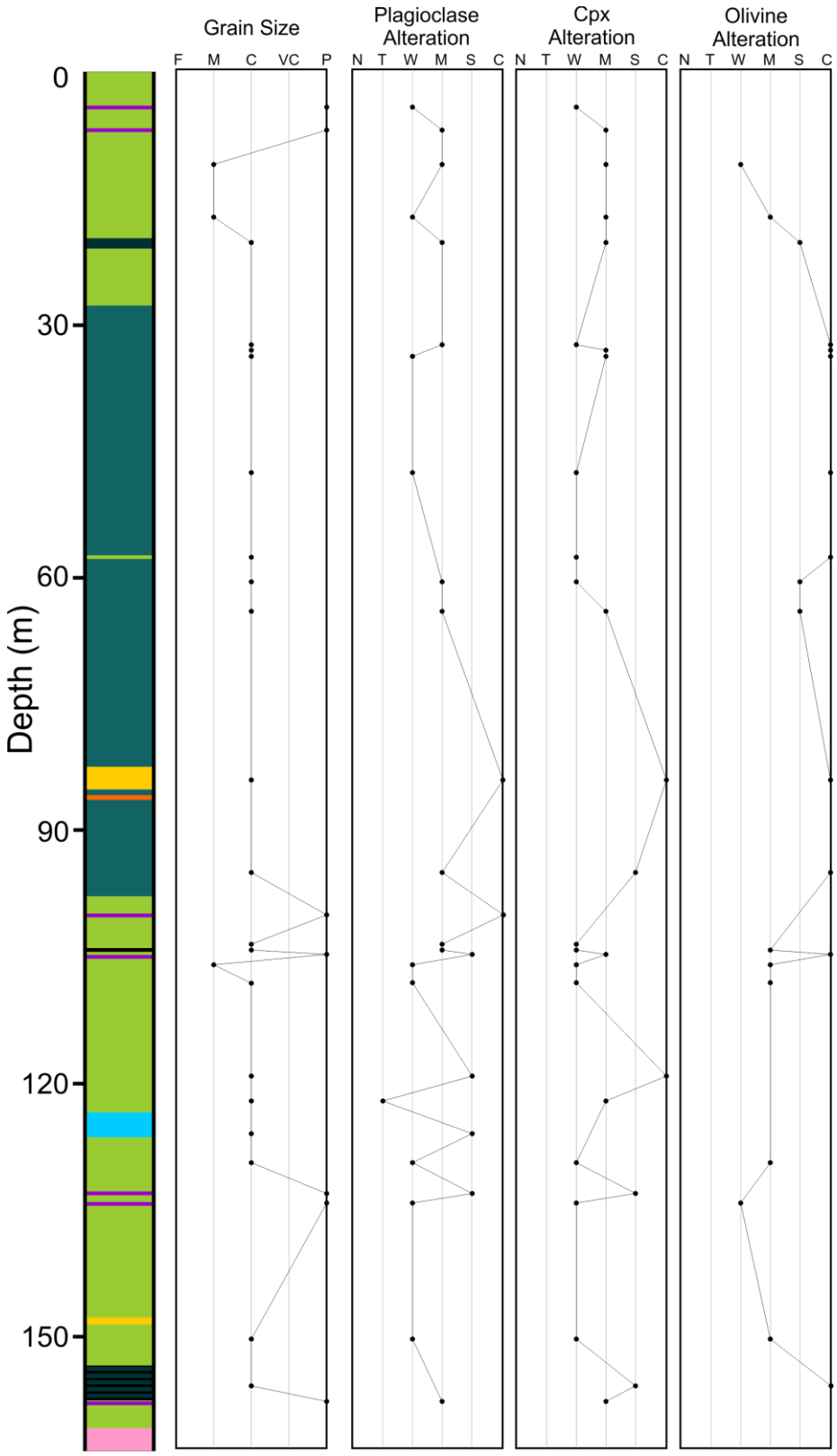

Figure 8: *Stratigraphic column of CL-06-39 showing variations in alteration. Grain sizes: Fine (F) = 0.8-1.5; Medium (M) = 1.5-3mm; Coarse (C) 3-7mm; Very coarse = 7-12mm.; Pegmatitic (P) = >12mm.*

Petrography of CL-06-16

Gabbro

Gabbroic units in CL-06-16 are primarily composed of plagioclase (25-50%) and clinopyroxene (20-55%), with variable amounts of olivine (0-10%). Plagioclase and clinopyroxene display subophitic textures and occasionally ophitic textures are present (Figure 9A,B). Inclusions of plagioclase are common in pyroxene and olivine throughout the entire section (Figure 9C). Plagioclase grains are euhedral-subhedral and display a wide range of sizes, from 0.02-5mm. Alteration of plagioclase is also quite variable where some grains only show trace amounts of sericite alteration and others display 80% alteration (Figure 10). Other alterations of plagioclase are chlorite and possible epidote. In intervals with heavily disseminated sulfide, plagioclase occurs as inclusions within pyrrhotite (Figure 9D). Clinopyroxene ranges in size from 0.05-7mm and are subhedral-anhedral. Exsolution lamellas of ilmenite along cleavage planes are present in all clinopyroxene grains and clinopyroxene occasionally contains inclusions of magnetite and ilmenite. Alteration products of clinopyroxene include amphibole (actinolite), biotite, chlorite, serpentine, and fine grained uralitization (Figure 11). The majority of alteration is present along the edges of grains, and typically where amphibole is in contact with clinopyroxene, the amphibole is altered to biotite and subsequently to chlorite. Biotite is also present as fine grained alteration product in the cores of clinopyroxene. Olivine, when present, is subhedral, highly fractured and ranges in size from 0.1-2mm. Fine grained (< 0.3mm) inclusions of plagioclase and ilmenite occur in olivine implying that olivine is a late cumulus phase. Samples near the top of the hole only show weak alteration of olivine to serpentine, while further downhole, complete olivine alteration to serpentine is present (Figure 11). Actinolite alteration is occasionally present on the edges of serpentine as well. Fine grained pyrite, as well as magnetite, can be present along fractures in olivine. Carbonate alteration is present in the gabbro and its occurrence is very patchy and generally localized around clinopyroxene, suggesting that the carbonate is an alteration product of clinopyroxene. (Figure 11).

Trace mineral phases that occur within gabbroic units include apatite, biotite, and amphibole. Biotite is present in three different forms; 1) corona around oxides, 2) interstitial grains to plagioclase and pyroxenes, and 3) poikilitic grains with inclusions of plagioclase and pyroxene (Figure 12A,B,C). Interstitial biotite grains are subhedral and < 0.4mm. Poikilitic grains are up to 5mm and contain < 1mm inclusions of euhedral plagioclase and subhedral pyroxene. Corona textured biotite is variable in thickness and may not always form a complete rim around the oxides. Total biotite content in gabbroic units can be up to 8%, but average is ~3%. Poikilitic amphibole also occurs with similar texture and appearance as the poikilitic biotite grains (Figure 12D). Apatite can be present up to 1% but typically occurs in trace amounts. Apatite grains are < 1.5mm but average ~0.2mm, are euhedral-subhedral, and occur interstitially to pyroxene and plagioclase (Figure 12E).

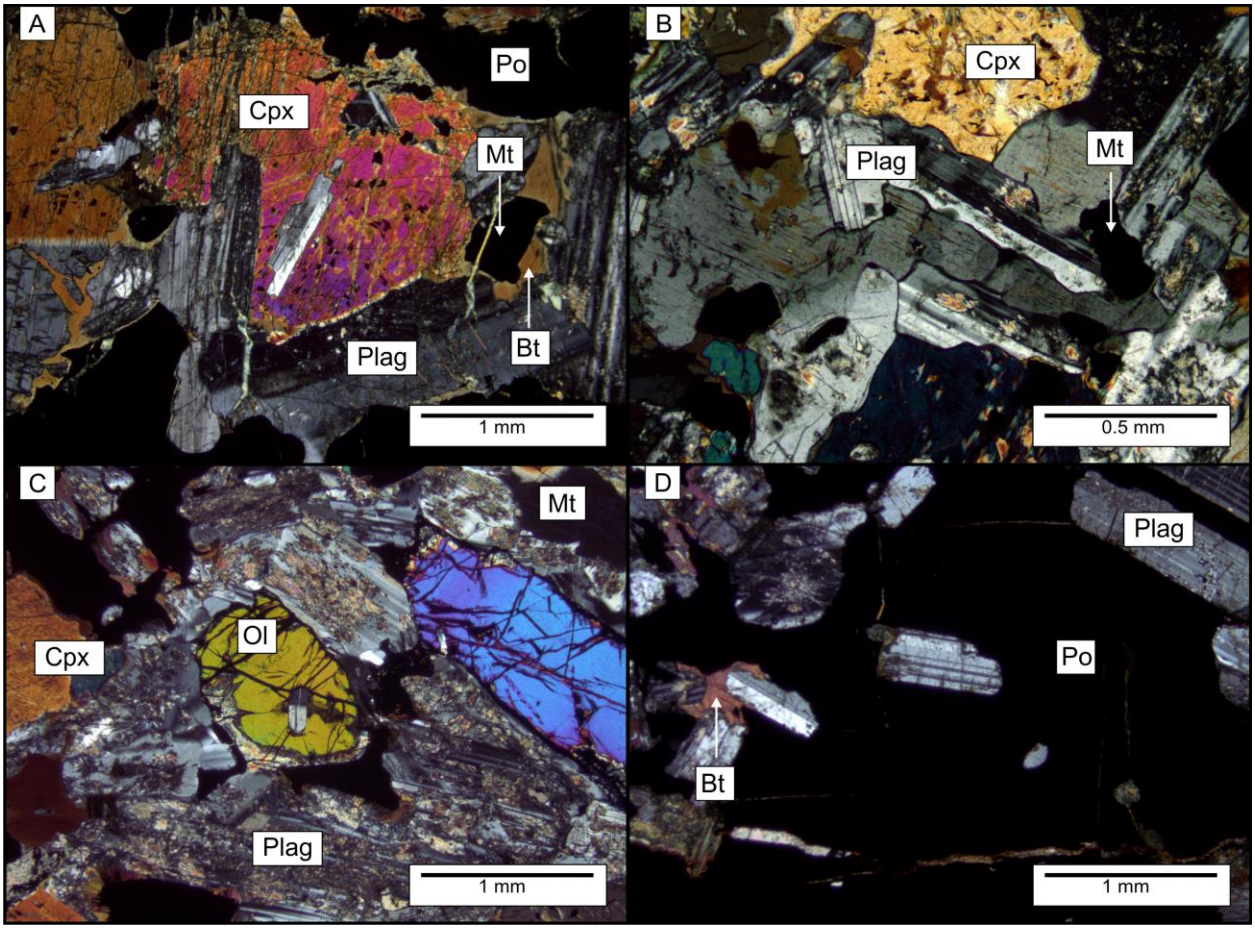

Figure 9: *Photomicrographs showing primary textures present in gabbro units in CL-06-16. A) Subophitic texture occurring between clinopyroxene (Cpx) and plagioclase (Plag). An inclusion of Plag occurs in Cpx as well. Small grains of magnetite (Mt) occur on the edge of Cpx and have a thin corona of biotite (Bt). Sample CL-06-16-57.5. Cross polarized light (XPL). B) Subophitic texture occurring between Cpx and Plag. Interstitial Mt occurs between Plag grains. Sample CL-06-16-59.9. XPL. C) Olivine (Ol) containing an inclusion of Plag. Magnetite occurs around the edge of Ol and interstitial to Plag and Cpx. CL-06-16-8.9. XPL. D) Plagioclase inclusion within highly disseminated pyrrhotite (Po). Fine-grained Bt occurs interstitial to Plag. CL-06-16-52.5. XPL.*

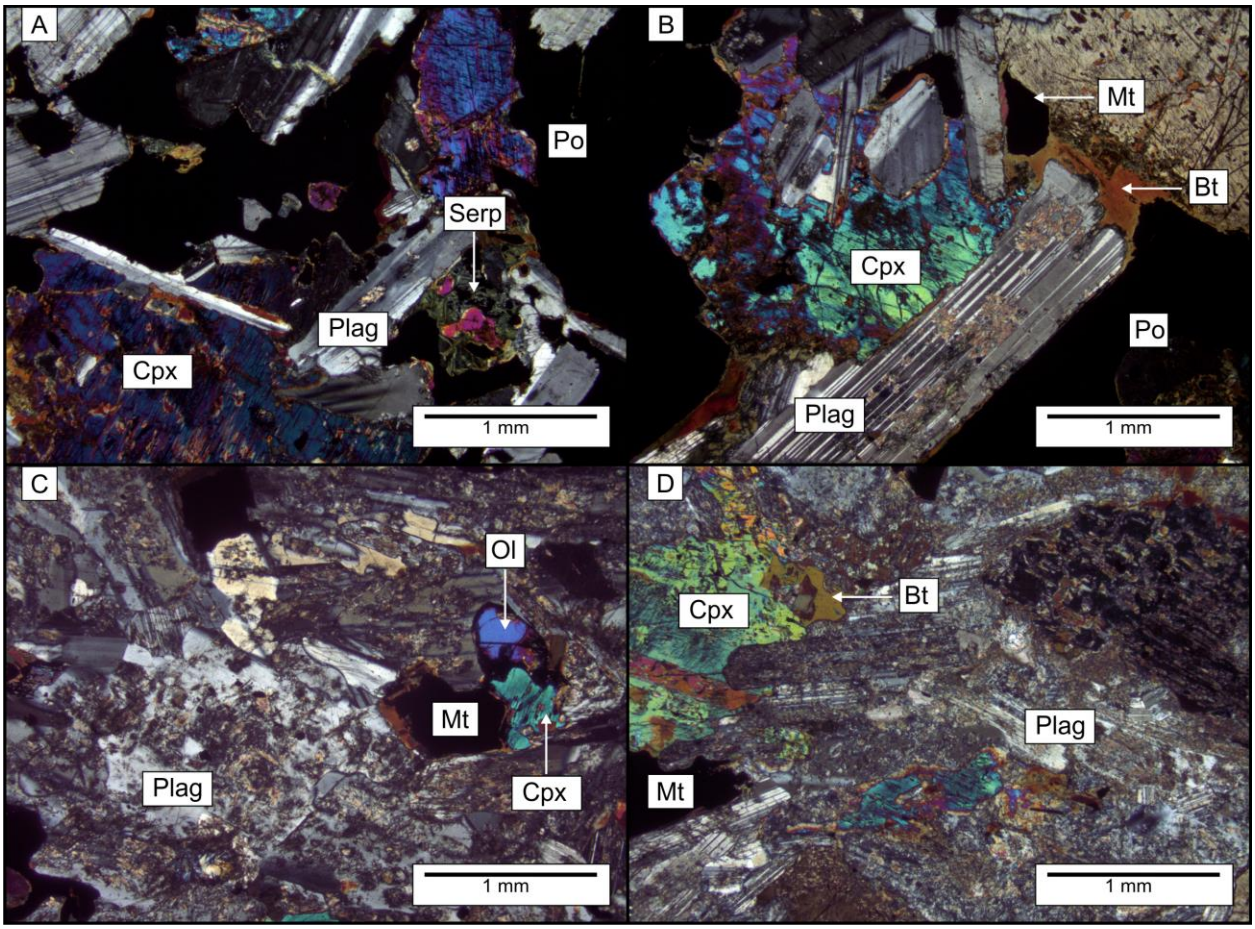

Figure 10: *Photomicrographs showing the range of alteration intensity demonstrated by plagioclase throughout the gabbro units in CL-06-16. A) Subophitic texture between Plag and Cpx. Plagioclase shows only trace amounts of alteration. Trace amounts of serpentine (Serp) are present with remnants of Cpx at its core. CL-06-16-56.3. XPL. B) Weak alteration of plagioclase with interstitial Bt and Mt between Plag and Cpx. CL-06-116-58.6. XPL. C) Moderate alteration of Plag. CL-06-16-8.9. XPL. D) Strong alteration of Plag. CL-06-16-11.2. XPL.*

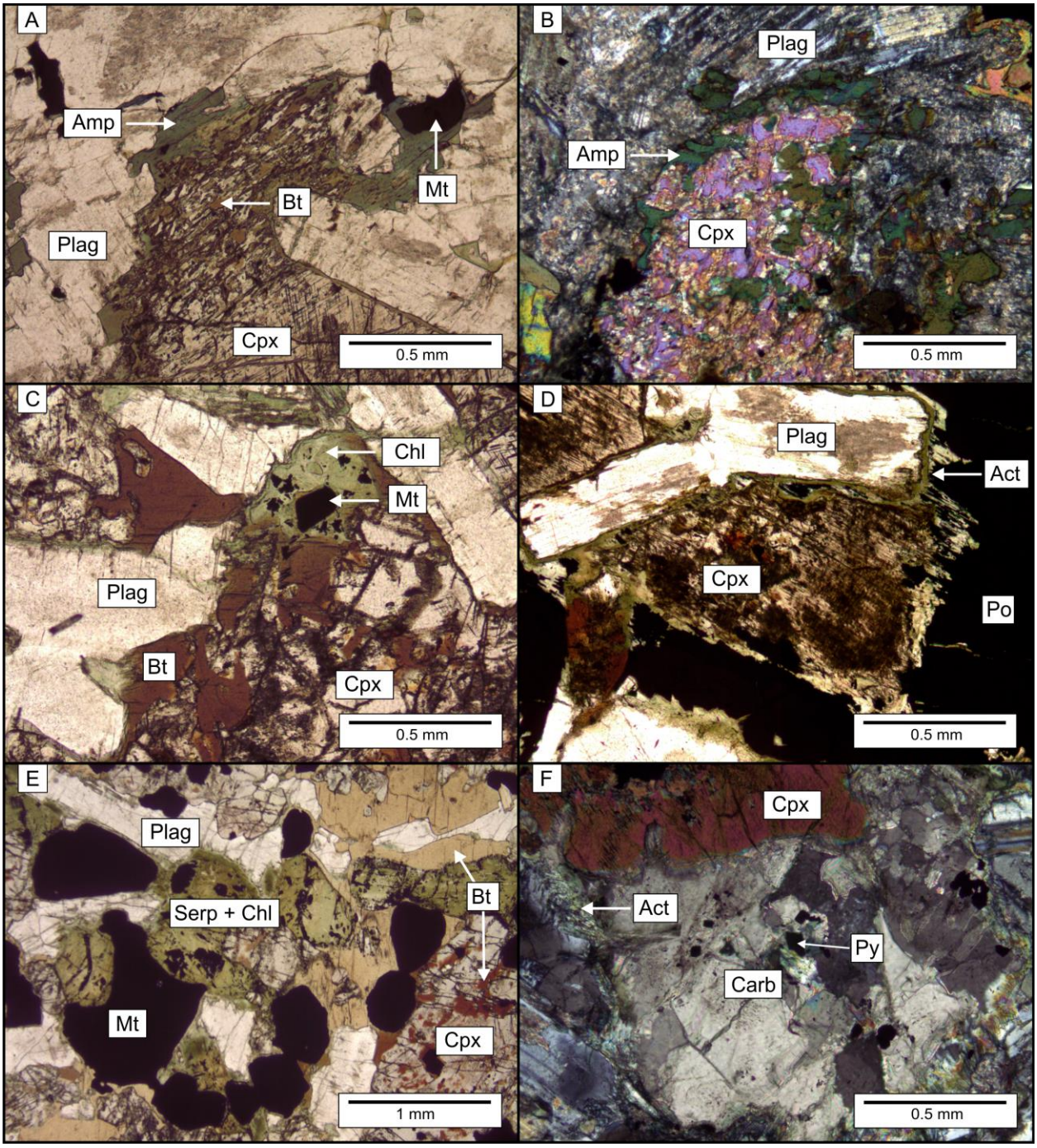

Figure 11: *Photomicrographs of alteration products of pyroxenes and olivine. A) Grain of Cpx that has an outer rim of amphibole alteration (Amp) and occurring inwards from the rim is fine grain Bt alteration. CL-06-16-52.5. Plane polarized light (PPL). B) Strong alteration of Cpx to Amp on the edge and appears to penetrate into the core of Cpx. CL-06-16-11.2. XPL. C) Moderate Bt alteration of Cpx at the core and along the rim with a patch of chlorite (Chl) with small inclusions of Mt. CL-06-16-56.3. PPL. D) Clinopyroxene and Plag have a rim of actinolite (Act) and the core has been altered to a very fine grained brown mineral (?). CL-06-16-63.8. PPL. E) Serpentine and Chl alteration olivine. CL-06016-55.0. PPL. F) Patch of carbonate (Carb) alteration next to a Cpx grain. A fine grained network of Act occurs along the rim of the Carb alt. CL-06-11.2. XPL.*

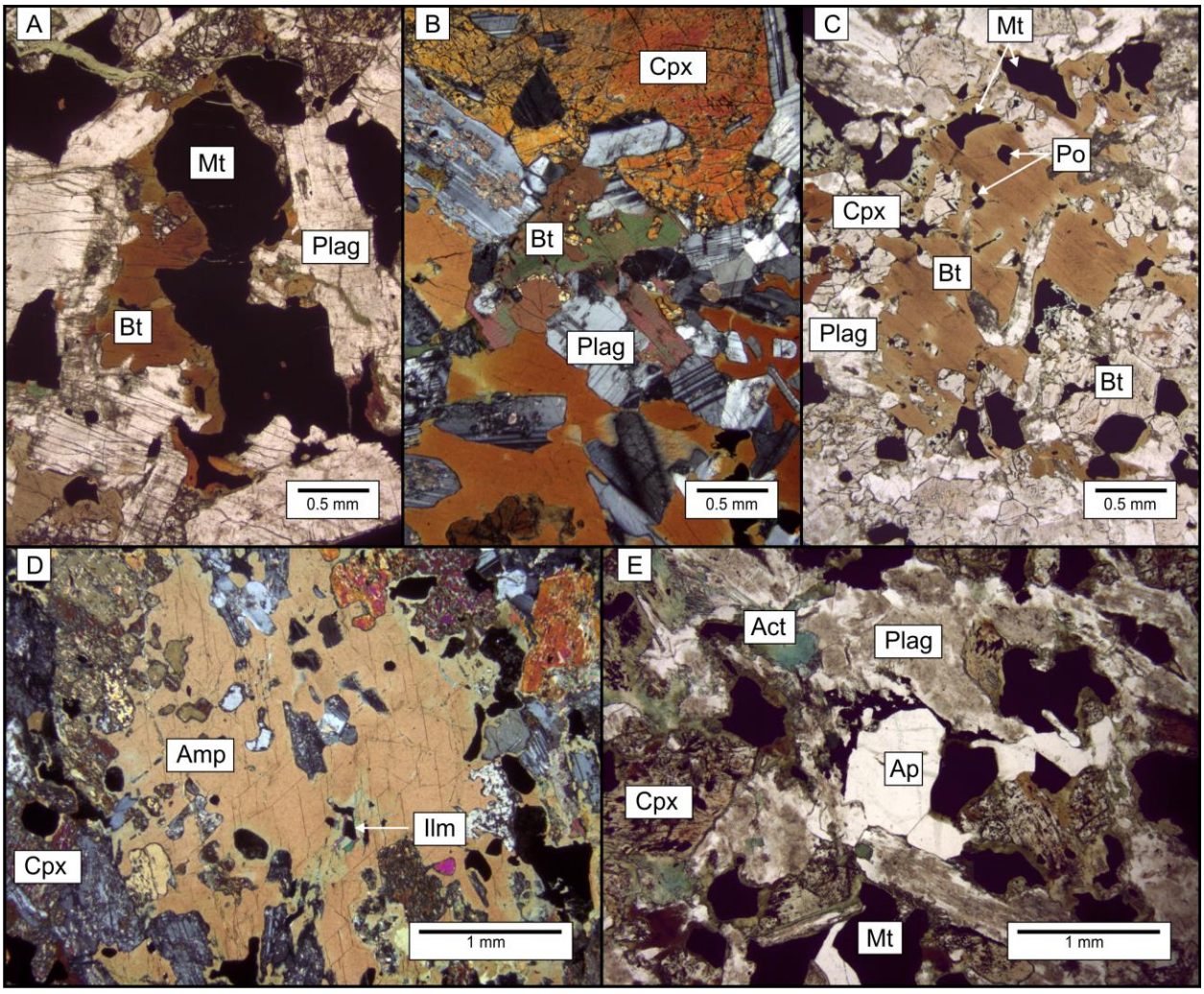

Figure 12: *Photomicrographs of trace to minor mineral phases present in the gabbro. A) Partial Bt corona on grain of magnetite. CL-06-16-57.5. PPL. B) Interstitial Bt to plagioclase grains. CL-06-16-56.3. XPL. C) Poikilitic Bt with inclusions of Cpx, Plag, Po, and Mt. CL-06-16-47. PPL. D) Poikilitic amphibole with inclusions of Plag, ilmenite (Ilm) and Cpx. CL-06-15-52.5. XPL. E) Interstitial apatite (Ap) to plagioclase. Interstitial Mt also occurs in close proximity to Ap. CL-06-16-63.15. PPL.*

Magnetite and ilmenite occur interstitially to silicates, comprising 2-12% of the gabbro and typically occur together as composite grains that are < 2.5mm. These composite grains are also found as inclusions within pyroxene and olivine. Two styles of exsolution are present within these composite grains, blebby exsolution where ilmenite exsolves to form a grain of its own on the edge of magnetite and trellis exsolution where ilmenite exsolves along a common plane (Figure 13 A,B). Magnetite always displays at least one style of exsolution but ilmenite can occur on its own but is not commonly observed. In sample CL-06-16-80.0, a graphic texture exists between ilmenite and feldspar, which likely indicates a eutectic crystallization of the two minerals (Figure 13C,D). Pyrrhotite is the dominate sulfide present within the gabbroic units comprising 1-25%. Detailed description of the disseminated sulfides is discussed below.

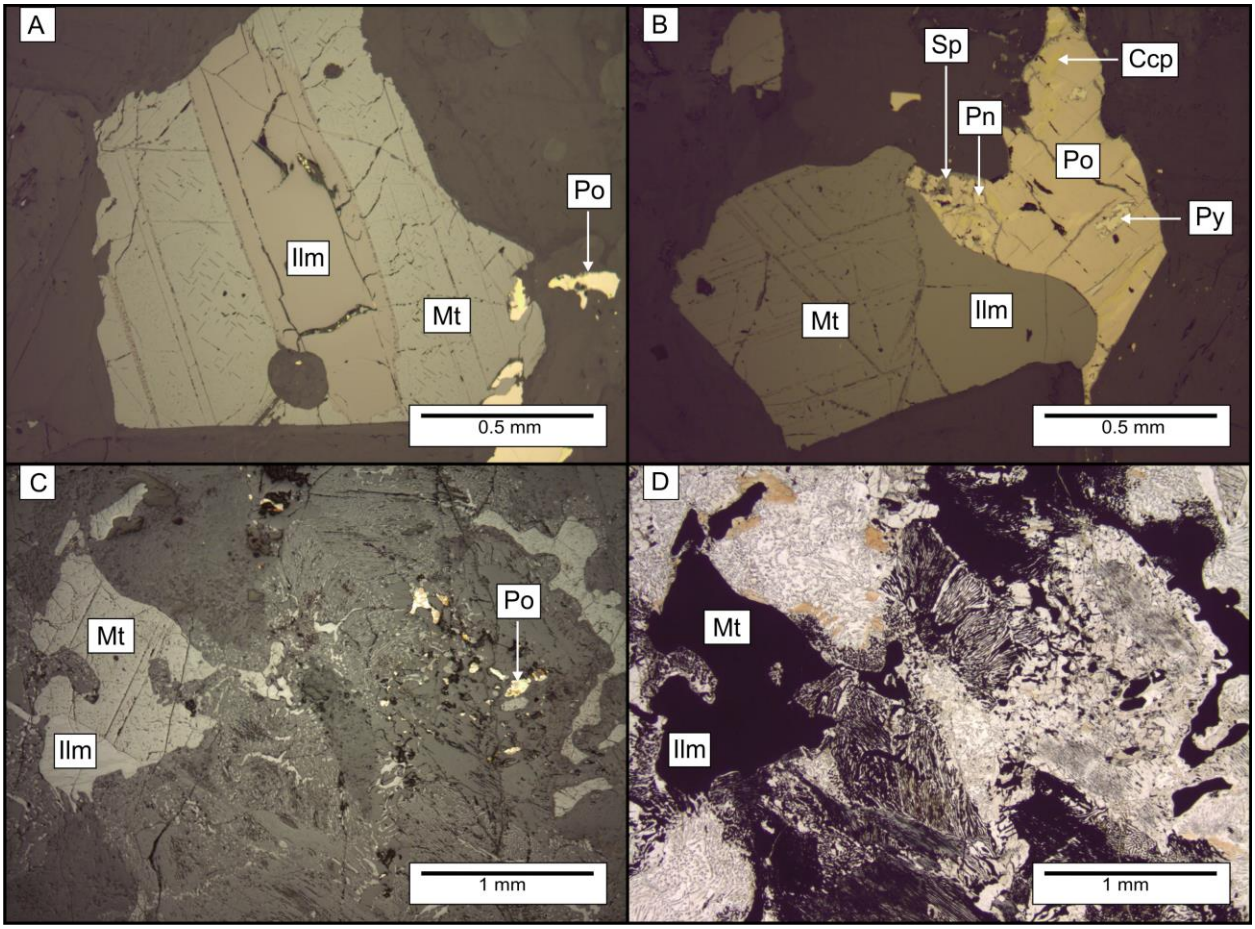

Figure 13: *Photomicrographs of oxide and sulfide phases in the feldspathic clinopyroxenite. A) Large trellis exsolution of ilmenite (Ilm) in Mt. Fine grained Po occurs near the edge of Mt. CL-06-16-35.7. RL. B) Trellis and blebby exsolution of Ilm from Mt. Grain of Po occurs on the edge of Ilm that contains inclusions of chalcopyrite (Ccp), sphalerite (Sp), pentlandite (Pn), and Py. CL-06-16-35.7. RL. C) Graphic texture occurs between an oxide (magnetite or ilmenite?) and feldspar. Blebby ilmenite exsolution occurs in the large grain of Mt. CL-06-16-80.0. Reflected light (RL). D) Same images as A, but in PPL.*

Clinopyroxenite

A small interval of clinopyroxenite consists primarily of clinopyroxene (50-75%) and lesser amounts plagioclase (5-10%), and olivine (0-15%). Clinopyroxene ranges in size from 0.3-7mm and is subhedral. Alteration of clinopyroxene is generally weak and consists of biotite starting to replace the edges of grains, with small patches of biotite occurring in the cores. Very fine grained (<0.3mm) inclusions of pyrite and ilmenite occur in clinopyroxene and ilmenite exsolution occurs along cleavage planes (Figure 14A). Inclusions of altered olivine also occur in clinopyroxene (Figure 14B). Clinopyroxene and plagioclase display an ophitic texture (Figure 13C). Plagioclase is 0.3-5mm, subhedral, and weakly-moderately altered to sericite. Anhedral inclusions of clinopyroxene and olivine occur in plagioclase (Figure 14D,E). Olivine is subhedral, highly fractured and ranges in size from 0.1-2mm. Very fine grained inclusions of ilmenite (< 0.4mm) occur in olivine as well as trace amounts of pyrite. Olivine is typically relatively unaltered, but some isolated grains have been completely replaced by serpentine and

chlorite (Figure 14B). Olivine is only present in the interval from 34.7-36.1m. Magnetite and ilmenite comprise 4-10% of the feldspathtic clinopyroxenite and are < 2.5mm in size.

Apatite is present in trace amounts up to 2% in the feldspathtic clinopyroxenite where it ranges in size from 0.05-1.5mm and is euhedral-subhedral. Apatite grains are interstitial to plagioclase and clinopyroxene, but apatite also occurs as inclusions within plagioclase suggesting it is an early phase (Figure 14F).

Similar to biotite in the gabbroic units, biotite in the clinopyroxenite occurs in trace amounts as coronas around oxides and as poikilitic grains with inclusions of plagioclase, oxides, and clinopyroxene. In the clinopyroxenite, magnetite, and ilmenite are commonly composite grains with two styles of exsolution. A rim of biotite is often found around these composite oxide grains. Up to 3% interstitial sulfides occur in the clinopyroxenite and predominantly consist of pyrrhotite with trace amounts of chalcopyrite, pentlandite, sphalerite, and pyrite. Sulfides are < 1.5mm with chalcopyrite occurring as very fine grained inclusions within pyrrhotite and pentlandite typically occurring as flame lamella in pyrrhotite and rare blocky form (Figure 13B).

Mineralization

Sulfide mineralization occurs in two different styles: 1) fine- to coarse-grained blebby disseminations that grades into a net texture (Figure 15A,B), and 2) massive (Figure 15C). Fine to coarse grained blebby disseminated sulfides occur in a fine to medium grained gabbros. The upper contact of the mineralized interval is with a fine grained gabbro that gradational increases in sulfide percentage downhole. Initially the unit contains trace sulfides then local concentrations of patchy pyrrhotite (~20%) occur, followed by 10-15% disseminated sulfides for approximately 2m, then the gabbroic unit is crosscut by a syenite dyke. After the dyke, sulfides comprise 20-30% of the unit and form a net texture until the lower contact, which is defined by a 1cm thick band of pyrrhotite. After the pyrrhotite band, the rock is a fine grained gabbro that contains only trace amounts of sulfide. Massive sulfide mineralization has either sharp upper and lower contacts with a fine to medium grained gabbro that contain ≤ 5% fine grained disseminated sulfides or has a short interval of net-textured sulfides above hosted by a medium grained gabbro.

Massive sulfide mineralization is primarily composed of pyrrhotite (~80%), with lesser amounts of chalcopyrite (2-10%), pentlandite (trace-3%), pyrite (trace), magnetite (5%), and ilmenite (trace), and sphalerite (trace). Pyrrhotite is massive and hosts all other minerals as inclusions. Chalcopyrite primarily occurs as anhedral inclusions within pyrrhotite that are ≤ 2mm (Figure 16A). In one instance, chalcopyrite occurs as a 4 mm wide veinlet crosscutting pyrrhotite and seems to be associated with a 5mm wide quartz veinlet that is also crosscutting pyrrhotite. Very fine grained (< 0.05mm) inclusions of sphalerite and pyrrhotite occur in both the chalcopyrite veinlet and in the anhedral chalcopyrite inclusions hosted by pyrrhotite (Figure 16A,B). Pentlandite occurs as flames in pyrrhotite and in a blocky form (Figure 16B,C). The blocky pentlandite is ≤ 0.1mm and is generally, but not always concentrated around anhedral chalcopyrite, as well on the form of pentlandite chains. Unlike blocky pentlandite, Flame pentlandite has no strong association with chalcopyrite and is ≤ 0.02mm.

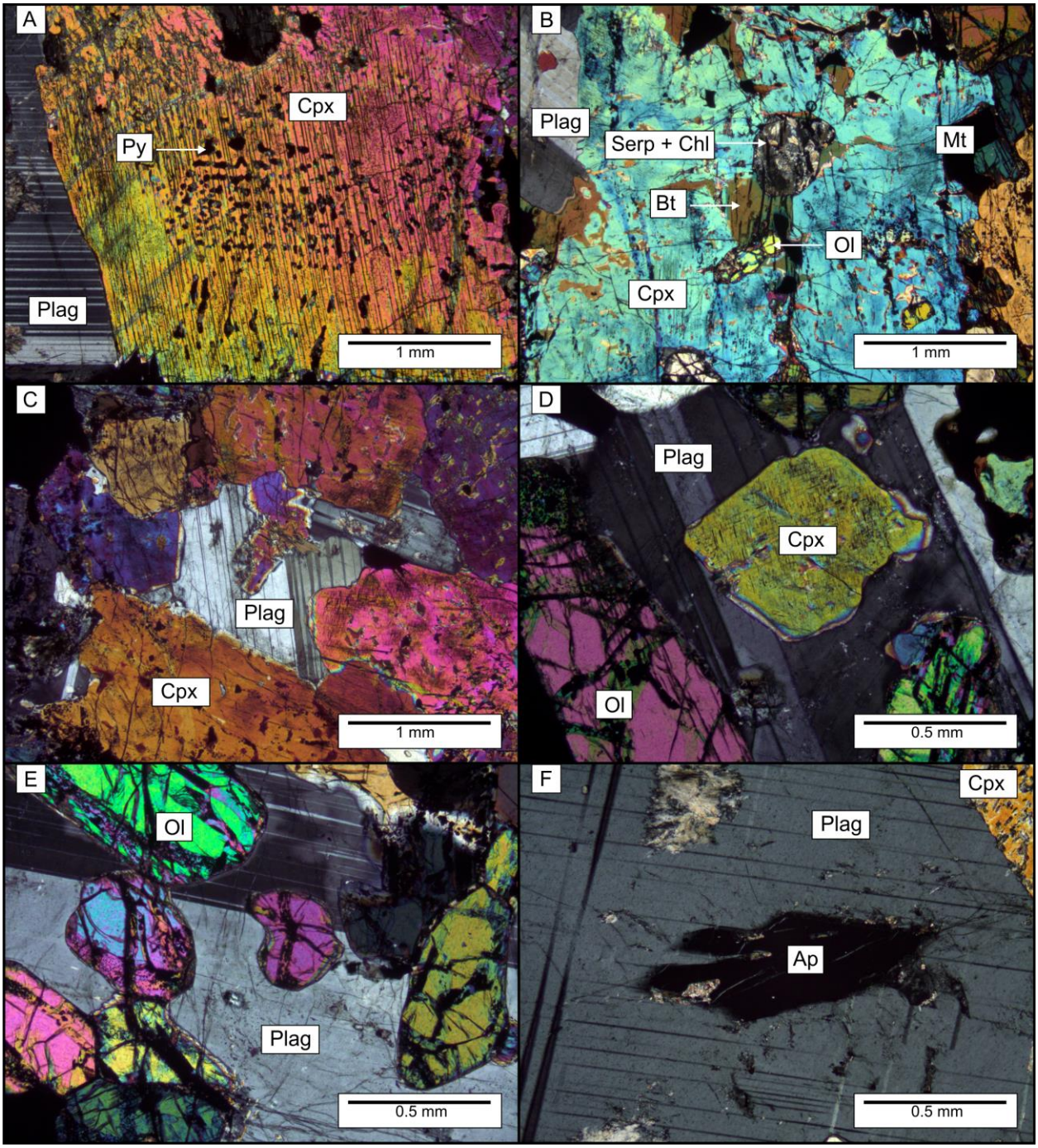

Figure 14: *Photomicrographs of primary textures and secondary alteration in the feldspathic clinopyroxenite. A) Fine grained inclusions of pyrite (Py) in Cpx. The Py inclusions resemble the outline of a grain and therefore Cpx may have overprinted a Py grain. CL-06-80.0. XPL. B) Large grain of Cpx that contains inclusions of non-altered Ol and Ol that has been altered to Chl and Serp. Biotite alteration is also present near the rims of Cpx and throughout the core. CL-06-16-35.7. XPL. C) Ophitic texture between Cpx and Plag. CL-06-16-35.7. XPL. D) Inclusion of Cpx within Plag. CL-06-16-35.7. XPL. E) Inclusions of Ol in Plag. CL-06-16-35.7. XPL. F) Inclusion of subhedral Ap within Plag. CL-06-16-80.0. XPL.*

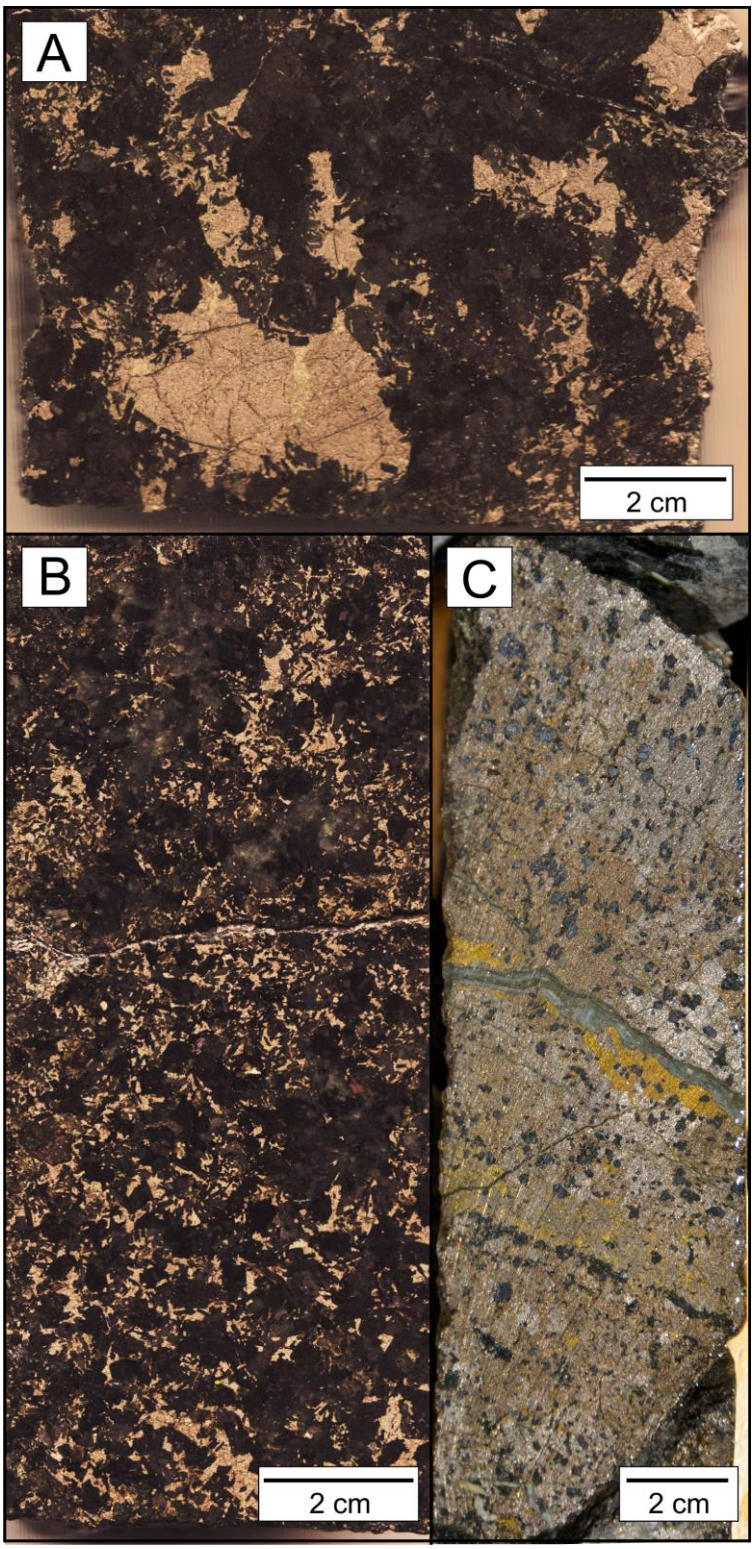

Figure 15: *Drill core slabs showing A) Medium to coarse grained Po and fine grained Ccp hosted in a fine to medium grained gabbro, CL-06-16-56.3. B) Fine grained disseminated to interstitial Po hosted in a fine to medium grained gabbro, CL-06-16-61.7. C) Massive Po with fine grained Ccp, Mt, and Ilm disseminated throughout. Chalcopyrite and Mt form linear features through the massive sulfide.*

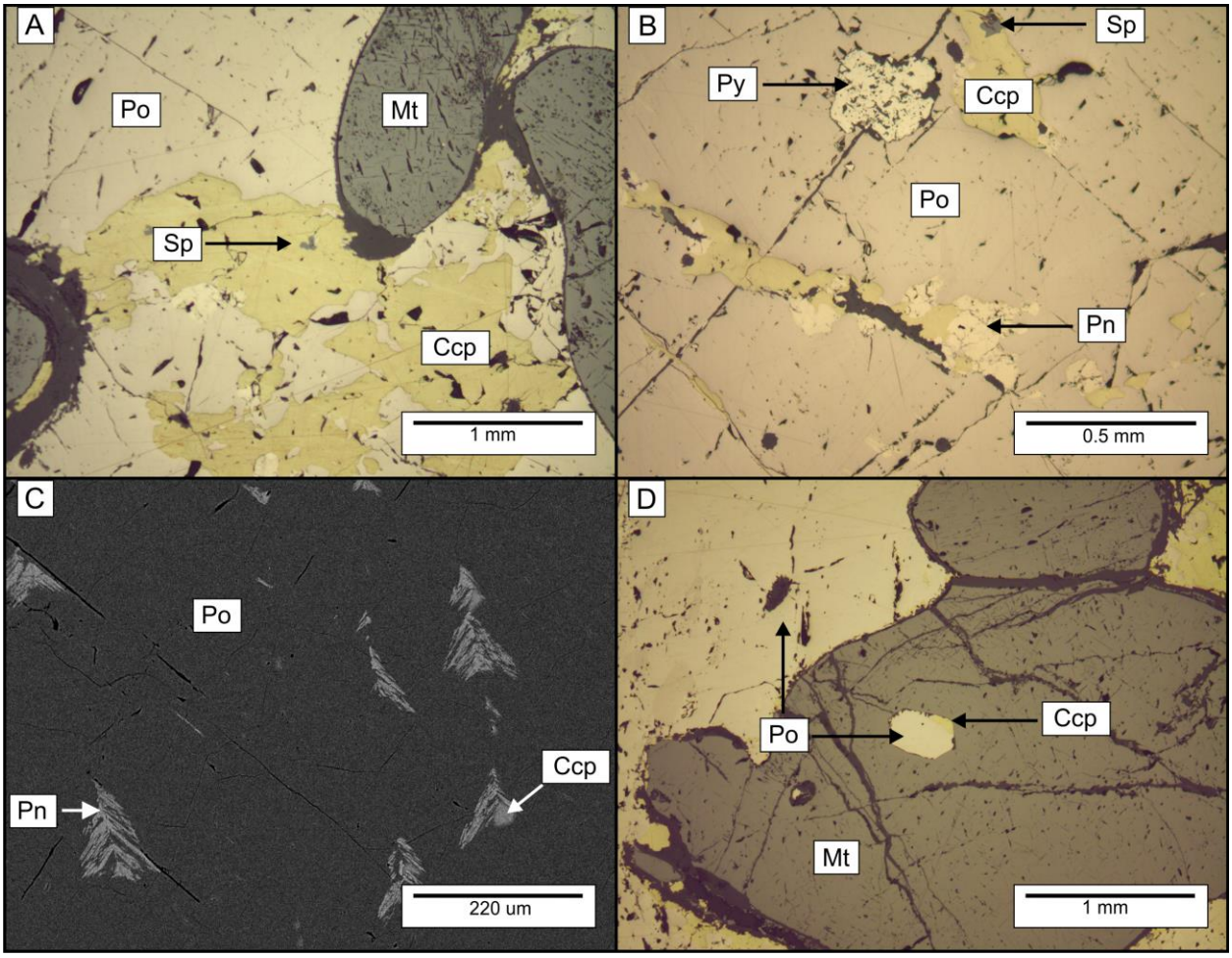

Figure 16: *Photomicrographs showing A) Anhedral inclusions of Ccp hosted in massive Po. Sphalerite occurs as small inclusions with Ccp. Magnetite exhibits a very thin exsolution texture comprised of ilmenite? Sample CL-06-05-81.6. RL. B) Anhedral inclusions of Ccp with blocky Pn concentrated around its edges and small grain of Sp. Pyrite replacement of Po occurs along a small fracture. Sample CL-06-05-81.6. RL. C) Back scattered image of Pn flames hosted in massive Po with blebby inclusions of Ccp. Sample CL-06-16-84.6. Backscatter electron image (BSE). D) Pyrrhotite inclusions with small grain of Ccp on the edge hosted in Mt that occurs as an inclusion within massive Po. Sample CL-06-05-81.2. RL.*

Blocky pentlandite comprises the majority volume of pentlandite present in the massive sulfide, while the flames only contribute a trace amount to the total percentage. Sphalerite grains are anhedral to blebby, ≤ 0.1mm and occur as inclusions within chalcopyrite and pyrrhotite or on the edges of chalcopyrite (Figure 16A, B). Pyrite is not observed as a primary sulfide mineral but as alteration of pyrrhotite. Grains of pyrite are typically concentrated along fractures, occur in a blocky form and are ≤ 0.2mm (Figure 16B). Magnetite occurs as 1-2.5 mm inclusions within pyrrhotite, typically blebby and moderately fractured. Pyrrhotite can occur as ≤ 0.5mm inclusions at the centre of magnetite grains. These small inclusions of pyrrhotite usually have a thin rim or small inclusions of chalcopyrite associated with them (Figure 16D). All magnetite grains display a very thin exsolution texture of ilmenite (Figure 16D). Very fine grained pyrrhotite and chalcopyrite is observed in fractures and along the edges of magnetite grains. In one instance observed it appears that pyrrhotite or pyrite is starting to alter magnetite.

Trace metal phases present in massive sulfide mineralization include galena, glaucodot-gersdorffite ((Co,Fe)AsS – NiAsS), molybdenite, nickeline, melonite ($NiTe_2$), electrum, and unidentified Se-Te-Pb, Bi-Te, and Pb-Te minerals that occur as inclusions within glaucodot-gersdorffite. Galena can occur as blebby to anhedral inclusions within pyrrhotite or as anhedral inclusions within glaucodot-gersdorffite grains. Glaucodot-gersdorffite occurs as inclusions within pyrrhotite or can be found along the edges of pyrrhotite at the contact with silicates or apatite (Figure 17A,B). Molybdenite tends to occur near fractures in pyrrhotite that have been infilled by quartz (Figure 17C). Nickeline, melonite and unidentified Se-Te-Pb and Te-Pb minerals were observed as inclusions within a single grain composed of an intermediate member of the glaucodot-gersdorffite solution forming the rim and a core composed of end-member gersdorffite (Figure 17D). One grain of electrum was observed and occurred as an anhedral inclusion within glaucodot-gersdorffite. The fashion that all the trace metal phases occur as (except galena) suggests that they are not primary in origin and related to a secondary mineralizing event.

Disseminated to net-textured sulfides/oxides constitute 10 – 25% of a fine to medium grained gabbro that is ~10.4m thick. Of the 10-25% of sulfides/oxides present, pyrrhotite represents 75-85%, magnetite (5-10%), ilmenite (5-10%), chalcopyrite (tr-5%), pyrite, (tr-3%), pentlandite (tr-1%) and sphalerite (tr). Pyrrhotite consists of angular interstitial grains that are ≤ 4mm (average 1mm) (Figure 18). Numerous euhedral plagioclase inclusions occur within pyrrhotite and range in size from 0.1 – 2mm. Inclusions of blebby magnetite and ilmenite are also present and range in size from 0.01-0.2mm. Chalcopyrite occurs as ≤ 1mm (0.1 mm) tabular to anhedral inclusions within pyrrhotite or occurs along the edges of pyrrhotite (Figure 18). Chalcopyrite that is not associated with pyrrhotite occurs as small (≤ 0.05mm) grains interstitial to plagioclase. Pentlandite occurs as flames and in a blocky form, similar to its occurrence in the massive sulfide mineralization (Figure 18). Grains of blocky and flame pentlandite are ≤ 0.02mm. Blocky pentlandite is commonly associated with chalcopyrite and/or near fractures within pyrrhotite and flame pentlandite occurs along fractures in pyrrhotite or at grain edges. Sphalerite is concentrated around chalcopyrite and is present as anhedral blebs that are ≤ 0.05mm (Figure 18). Pyrrhotite can be found as inclusions within sphalerite, but is rare to observe. Some grains of sphalerite display chalcopyrite disease. Blocky pyrite occurs as a replacement texture of pyrrhotite and is concentrated along fractures (Figure 18). Grains of pyrite are ≤ 0.5mm (0.1mm). Magnetite and ilmenite generally occur as composite grains featuring blebby and trellis styles of exsolution (Figure 18), typically ≤ 4mm (1mm). Composite grains are observed with either magnetite or ilmenite comprising the core and the other occurring at the edge. Individual magnetite and ilmenite grains are typically ≤ 0.5mm. Inclusions of pyrrhotite, ≤ 0.2mm, occur in ilmenite/magnetite and commonly have a thin rim of chalcopyrite (Figure 18). Only minor amounts of trace metal bearing phases have been observed in the disseminated to net-textured sulfides and consist of anhedral glaucodot-gersdorffite and blebs of galena as inclusions within pyrrhotite. One grain of cassiterite was found and occurred as an inclusion within plagioclase.

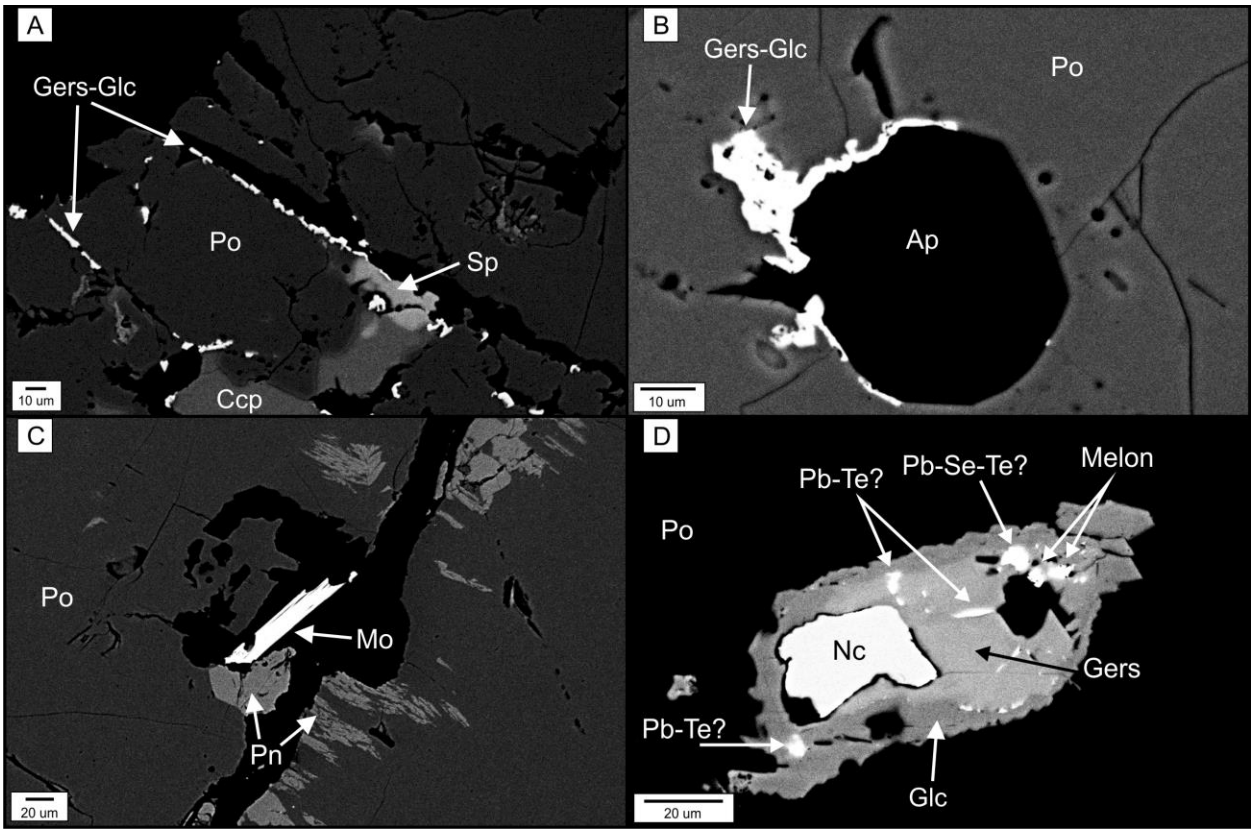

Figure 17: *SEM-BSE photomicrographs showing trace mineral phases present in massive sulfide. A) Gersdorffite-glaucodot (Gers-Glc) fine grained blebs that occur on the edge of Po and Ccp. Sphalerite is present on the edge of Po and Ccp as well. CL-06-16-81.6. BSE. B) Anhedral Gers-Glc occurring along the contact of Po and Ap. CL-06-16-84.6. BSE. C) Tabular grain of molybdenite (Mo) occurring along a fracture. Blocky and flame Pn occur on the edges of the fracture as well. CL-06-16-84.6. BSE. D) Zoned grain of gersdorffite-glaucodot, where the rim is an intermediate composition of the two minerals and the core is end-member gersdorffite. Blebby inclusions of melonite (Mel), nickeline (Nc) and unidentified Pb-Te and Pb-Se-Te minerals occur within the grain. CL-06-16-84.6. BSE.*

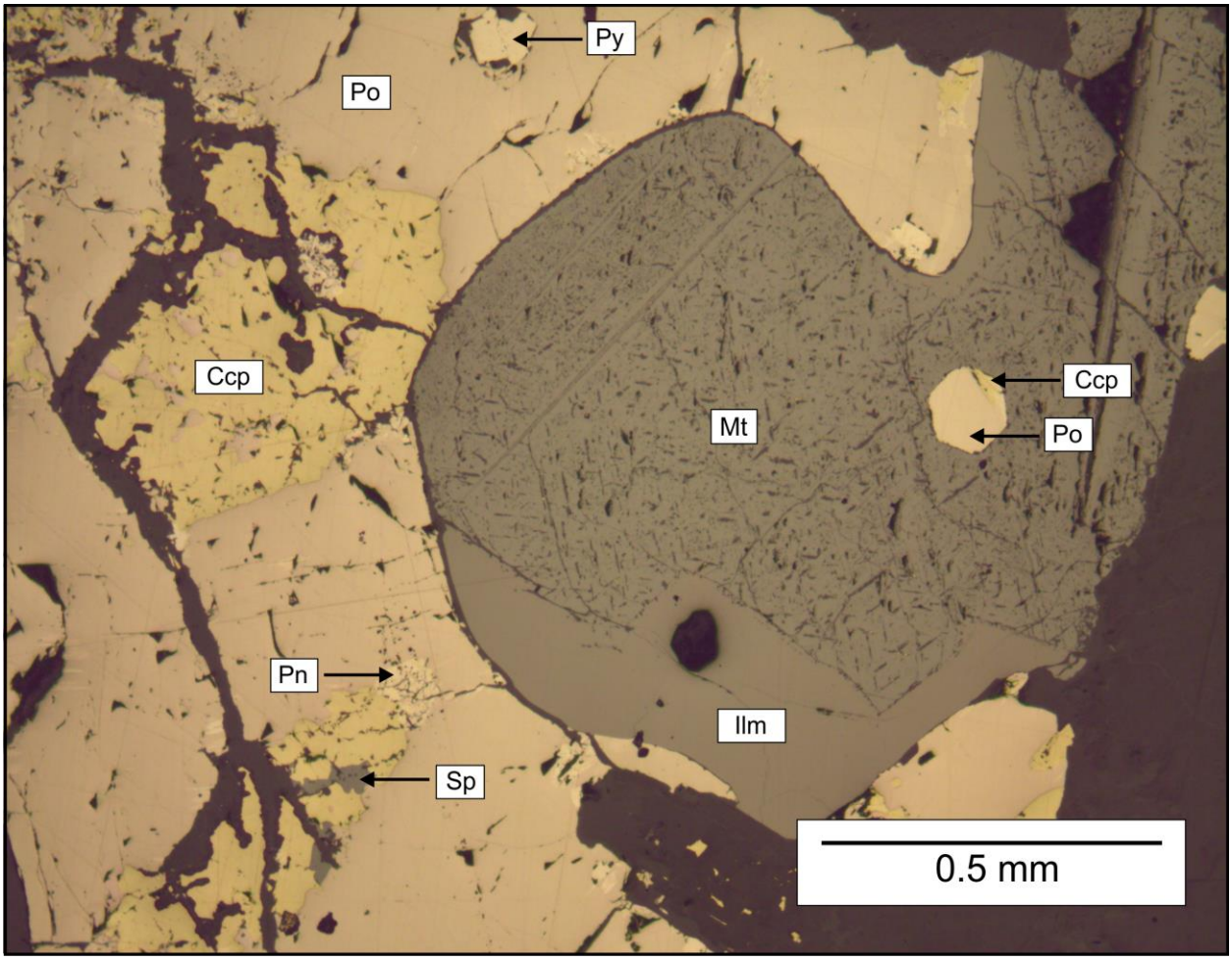

Figure 18: *Photomicrograph showing disseminated Po containing anhedral Ccp inclusions. Chalcopyrite contains inclusions of Po and Sp occurs along the grain boundaries of Ccp and Po grains. Pentlandite is present at the edge of Ccp in a blocky form and as fine flame lamella in Po. Pyrite replacement of Po is also present. Magnetite and Ilm compose a composite grain with Ilm occurring on the edge and Mt at the core. Magnetite displays a trellis pattern with Ilm exsolution. Within Mt, a blebby inclusion of Po occurs that has a partial rim of Ccp. Sample CL-06-16-58.6. RL.*

Geochemistry

Rocks of the CLI are of alkaline to sub-alkaline affinity and follow a tholeiitic trend (Figure 19). Chondrite-normalized plots of unaltered fine grained gabbros within the CLI display a negative slope, with a moderate enrichment in the light rare earth elements (LREE) over the heavy rare earth elements (HREE); (Figure 20A). Both the unaltered and altered fine grained both have similar LREE enriched profiles with a positive Eu anomaly (Figure 20A). Primitive mantle normalized plots of the unaltered fine grained gabbros show a slight enrichment in Sr and Ti, likely due to Plagioclase and ilmenite respectively (Figure 20B). Both altered and unaltered gabbros show depletions in Th, U, and HREE. Altered fine grained gabbros are highly enriched in Pb compared to unaltered gabbros, and show moderate enrichments in Cs and Rb, while being slightly depleted in some LREE (Figure 20B). Pegmatites plotted on a chondrite normalized plot also follow the same trend as unaltered fine grained gabbros, except for one sample (CL-07-05-499) (Figure 21A). Primitive mantle normalized plots of the pegmatites exhibit similar patterns

to those of the grained gabbros (Figure 21B). Only a few minor enrichments, such as Pb, Rb, Ba, and Cs are noted.

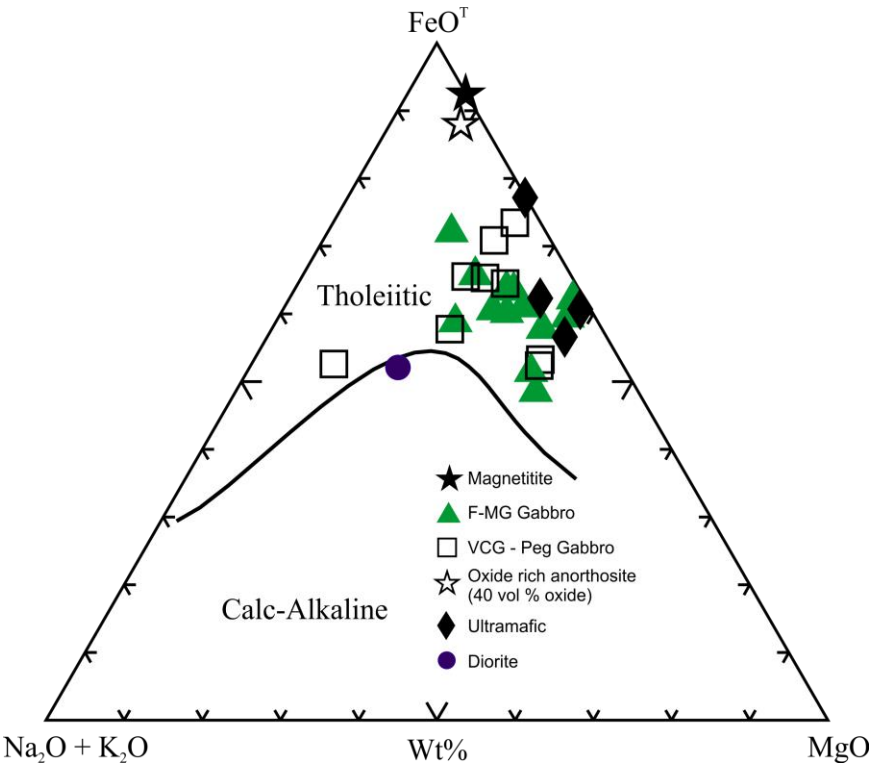

Figure 19: *AFM diagram (after Irvine and Barager, 1971) of rocks from the Caribou Lake Intrusion show that they are of a tholeiitic composition and as the melt evolved, rocks move away from the FeO-MgO tie line. F-MG Gabbro = Fine-medium grained gabbro. VCG-pegmatitic gabbro = Very coarse grained – pegmatitic gabbro. FeO^T = total Fe.*

Gabbroic rocks in the intrusion show similar SiO_2 contents (39-45 wt%) with each other regardless of their relative position in drill core. Typically, the gabbros with higher SiO_2 are a function of higher alteration present in the sample and Al_2O_3 also follows this trend. Magnetite and ilmenite are a direct control on the FeO and TiO_2 content of gabbros. As units with higher FeO and TiO_2 (15-18 and 2.6-4.2 wt%, respectively) contain 5-12% Fe-Ti oxides, while gabbros with lower amounts of Fe-Ti oxides (2-3%) have FeO and TiO_2 contents of ~11 and ~1.5 wt%, respectively. Ultramafic rocks (dunite, clinopyroxenite) have MgO concentrations of 13-18 wt% and highly variable FeO and TiO2 (22-51 and 2-8 wt% respectively) contents controlled by Mag and ilmenite. Vanadium concentrations are highly variable, ranging from 50 ppm up to 2.3 wt% averaging ~500 ppm. Geochemical results from the preliminary sample set collected in February 2013 are presented in Appendix C.

Nickel sulfide fire assay results of the samples collected in February 2013 returned marginal results for PGE and Au. Highest Pd and Pt concentrations, 6.72 and of 7.68 ppb respectively, occurred in a very coarse grained gabbronorite (CL-07-14-477.5). The highest Au content was observed in a clinopyroxenite (CL-07-05-50) 21.3 ppb. Full PGE and Au results are listed in Table 1.

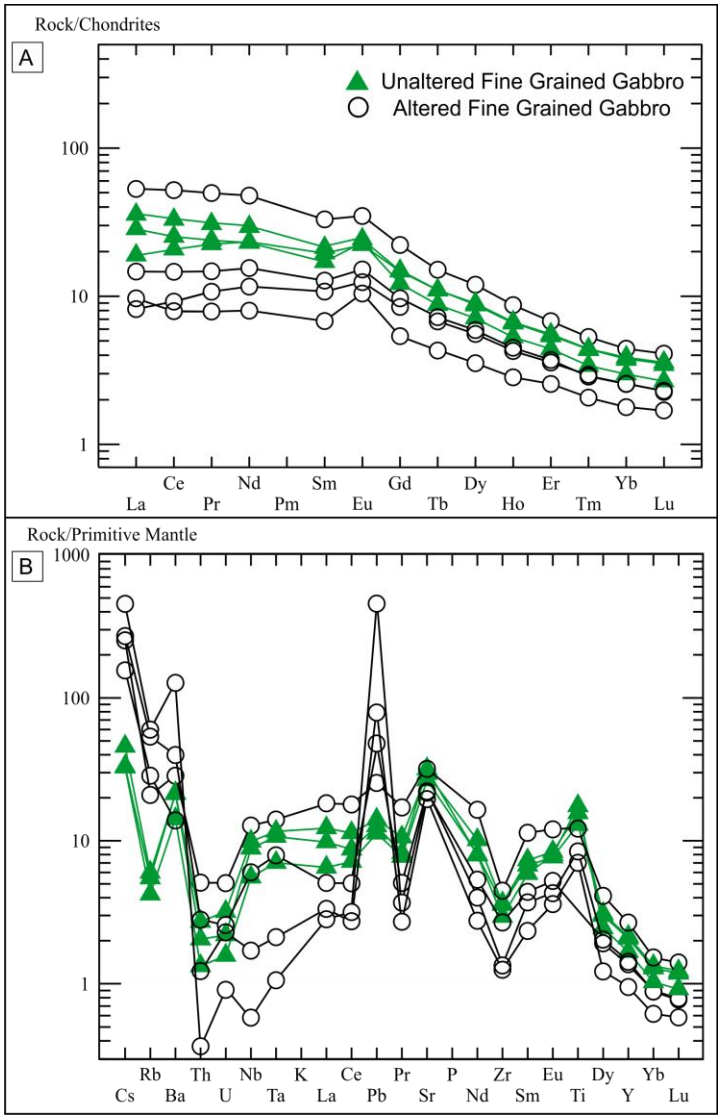

Figure 20: *A) Chondrite normalized plot comparing unaltered and moderately to highly altered fine grained gabbros. Both show the same negative slope and a positive Eu anomaly. B) Normalized primitive mantle plot comparing same unaltered and altered fine grained gabbros as in A. Both show similar trends in trace elements, except for Pb, which is highly enriched in the altered samples. After Sun and McDonough, 1989.*

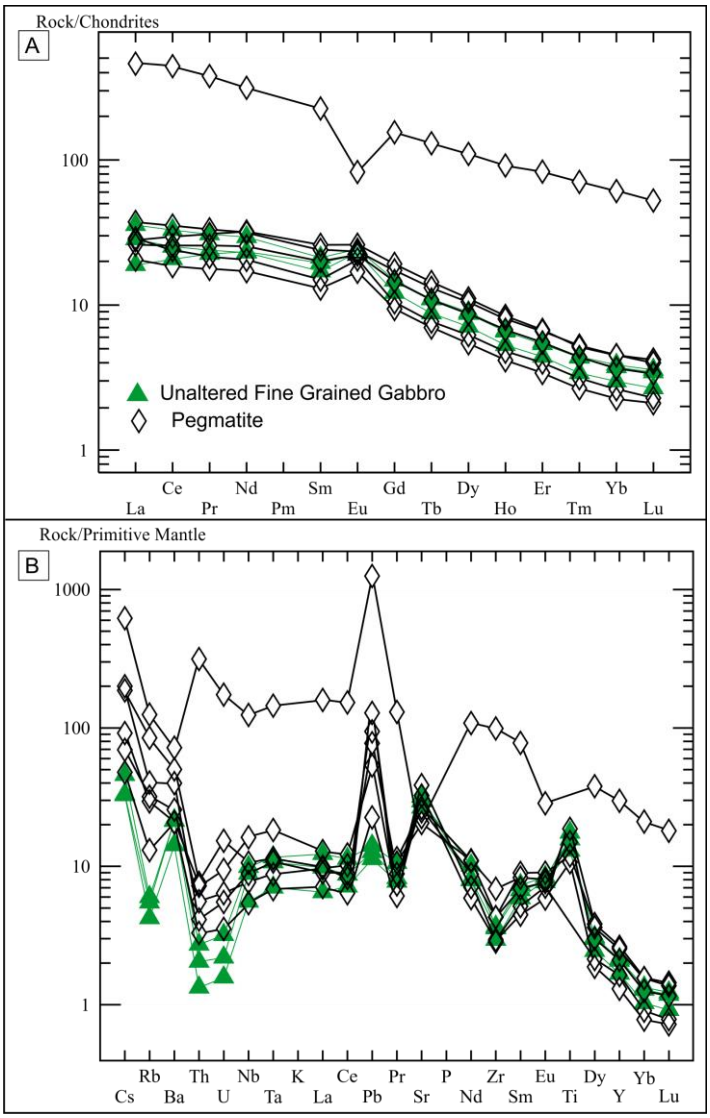

Figure 21: *A) Chrondrite normalized plot of unaltered fine grained gabbros compared to pegmatitic gabbros. All but one sample follows the same trend as the fine grained gabbros. The outlier (CL-07-05-499) is highly enriched in all REE and exhibits a negative Eu anomaly rather than a positive anomaly. B) Normalized primitive mantle plot for same units as in A. Pegmatites have a slight enrichment in Pb compared to the unaltered gabbros. Again, the one sample is highly enriched in its trace elements compared to unaltered gabbros. After Sun and McDonough, 1989.*

Sulfur Isotopes

Sulfides from 26 samples from the CLI representing primary and secondary generations of sulfide formation as well as pyrrhotite from the Burwash formation were analyzed by Isotope Ratio Mass Spectrometery (IRMS) and by Secondary Ion Mass Spectrometery (SIMS) for their sulphur isotopic composition. Primary sulfides analyzed consisted of pyrrhotite and chalcopyrite occurring in various styles; semi-massive to massive, disseminated, and inclusions within olivine and ilmenite. The secondary sulfides analyzed were pyrrhotite and pyrite, which were either hosted along fractures, associated with alteration, or present as a late stage veinlet crosscutting the sample. Sulfur isotopes from three samples, CL-07-01-373, CL-06-05-77.72, and CL-06-35-

56.36 were analyzed by SIMS. Within CL-07-01-373, three different styles of pyrrhotite were analyzed; inclusions hosted in olivine and ilmenite, interstitial to clinopyroxene and moderately altered plagioclase, and secondary pyrrhotite associated with actinolite alteration. A secondary pyrrhotite stringer was analyzed in CL-06-05-77.72, and pyrrhotite from CL-06-35-56.36 representing the Burwash Formation was analyzed.

Interstitial and disseminated pyrrhotite had an average $\delta^{34}S$ of 0.8 ± 0.5 ‰ (n= 16 by IRMS ; n=7 by SIMS) (Figure 22A; Figure 23). Pyrrhotite inclusions in ilmenite and olivine had average values of 0.2 ± 0.6 ‰ (n=7) and 0.3 ± 0.5 ‰ (n= 8), respectively (Figure 22B, C; Figure 23). Sulfur isotopic values of semi-massive to massive sulfides were 1.2 ± 0.1 ‰ (n= 6). Secondary pyrrhotite associated with alteration had $\delta^{34}S$ values of 0.9 ± 0.2 ‰ (n= 7) (Figure 22D). Fracture hosted pyrite associated with serpentine had isotopic values of 0.7 ±0.1 ‰ (n= 2). A late pyrrhotite stringer crosscutting a fine to medium grained gabbro gave a $\delta^{34}S$ value of 2.5 ‰ when analyzed by IRMS, and was also analyzed by SIMS, giving values of 0.6 ± 1 ‰ (n = 7). Pyrrhotite from the Burwash Formation have values ($\delta^{34}S$ = 0.2 ± 0.4 ‰) similar to all the other styles of sulfides. Full sulfur isotope results are listed in Table 2 and ranges in $\delta^{34}S$ values are plotted in Figure 23.

Table 1: *Ni-sulfide PGE fire assay results.*

Sample	CL-07-01-8	CL-07-01-115.7	CL-07-01-167.76	CL-07-01-322.4	CL-07-01-325.6	CL-07-01-354.2
Rock Type	Diorite	Gabbro	Pegmatitic Gabbro	Oxide rich Anorthosite	Gabbro	Gabbro
S (wt%)	0.02	0.38	0.14	0.3	0.25	0.55
Au (ppb)	<0.22	1.82	0.48	0.76	0.65	1.05
Ir	0.01	0.14	0.01	0.01	0.01	0.06
Pd	<0.12	1.72	0.15	0.15	<0.12	1.01
Pt	<0.17	1.24	0.27	0.23	<0.17	0.9
Rh	<0.02	0.07	<0.02	<0.02	<0.02	0.08
Ru	<0.08	0.25	<0.08	<0.08	<0.08	0.1

Sample	CL-07-01-371.2	CL-07-01-373	CL-07-01-380	CL-07-01-422.9	CL-07-02-347	CL-07-03-169
Rock Type	Gabbro	Olivine Gabbro	Gabbro	Gabbro	Gabbro	Gabbro
S (wt%)	0.27	0.31	0.23	0.8	0.36	0.1
Au (ppb)	0.44	0.5	0.74	0.41	0.72	0.93
Ir	0.02	0.02	0.01	0.11	0.02	0.13
Pd	0.16	0.2	<0.12	2.22	0.24	0.77
Pt	<0.17	<0.17	<0.17	3.72	<0.17	0.69
Rh	0.02	<0.02	<0.02	0.13	<0.02	0.07
Ru	<0.08	<0.08	<0.08	0.21	<0.08	0.24

Sample	CL-07-05-11	CL-07-05-14	CL-07-05-30.2	CL-07-05-50	CL-07-05-105	CL-07-05-117
Rock Type	Dunite	Gabbro	Gabbro	Clinopyroxenite	Gabbro	Dunite
S (wt%)	0.35	0.45	0.27	1.27	0.23	0.46
Au (ppb)	6.81	4.34	0.23	21.3	0.45	12.5
Ir	1.74	0.16	0.01	1.99	0.01	1.3
Pd	5.83	0.74	<0.12	5.74	<0.12	4.98
Pt	5.59	0.9	<0.17	1.82	<0.17	3.02
Rh	0.85	0.09	<0.02	1.01	<0.02	0.64
Ru	3.67	0.33	<0.08	3.95	<0.08	2.49

Sample	CL-07-05-142.8	CL-07-05-144	CL-07-05-499	CL-07-05-675	CL-07-07-10.1	CL-07-07-17
Rock Type	Olivine Gabbro	Olivine Gabbro	Gabbro	Magnetitite	Gabbro	Gabbro
S (wt%)	0.75	0.7	0.97	0.09	0.35	0.41
Au (ppb)	10.2	15	1.05	0.63	0.38	0.47
Ir	0.42	0.36	0.01	0.03	0.01	0.02
Pd	3.27	3.94	<0.12	0.26	<0.12	0.13
Pt	3.16	3.61	<0.17	<0.17	<0.17	<0.17
Rh	0.26	0.23	<0.02	0.03	<0.02	0.02
Ru	0.58	0.52	<0.08	0.13	<0.08	<0.08

Sample	CL-07-07-450	CL-07-07-483	CL-07-14-323.5	CL-07-14-477.5	CL-07-15-145
Rock Type	Gabbro	Gabbro	Gabbro	Gabbro	Gabbro
S (wt%)	0.3	0.15	0.59	1.6	0.02
Au (ppb)	0.42	0.4	2.29	15.7	<0.22
Ir	0.01	0.01	0.08	0.81	0.01
Pd	<0.12	<0.12	0.6	6.72	<0.12
Pt	<0.17	<0.17	2.58	7.68	<0.17
Rh	<0.02	<0.02	0.05	0.51	<0.02
Ru	<0.08	<0.08	0.14	1.44	<0.08

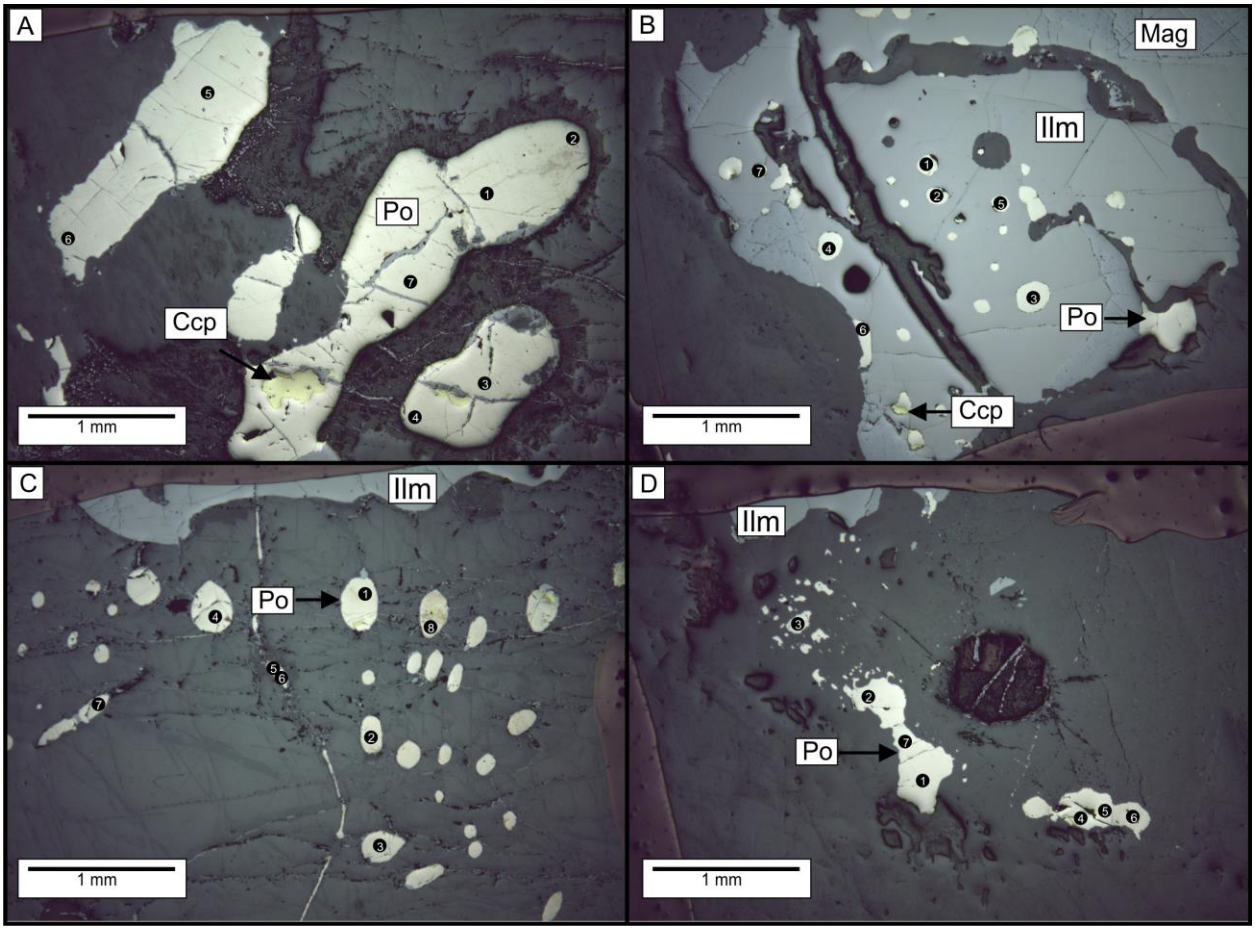

Figure 22: *Photomicrograph of Sample CL-07-01-373 in RL showing different sulphide textural styles analyzed by SIMS. A) Interstitial Po with Ccp inclusions, B) Inclusions of Po in Ilm. Pyrrhotite grains may have thin rim of Ccp at contact with Ilm, and may be sulfide melt inclusions C) Inclusions of Po hosted within Ol (with other minor phases, constitute sulfide melt inclusions). D) Interstitial Po that is surrounded by actinolite alteration. Numbers in images represent corresponding* $\delta^{34}S_{CDT}$ *values in Table 2.*

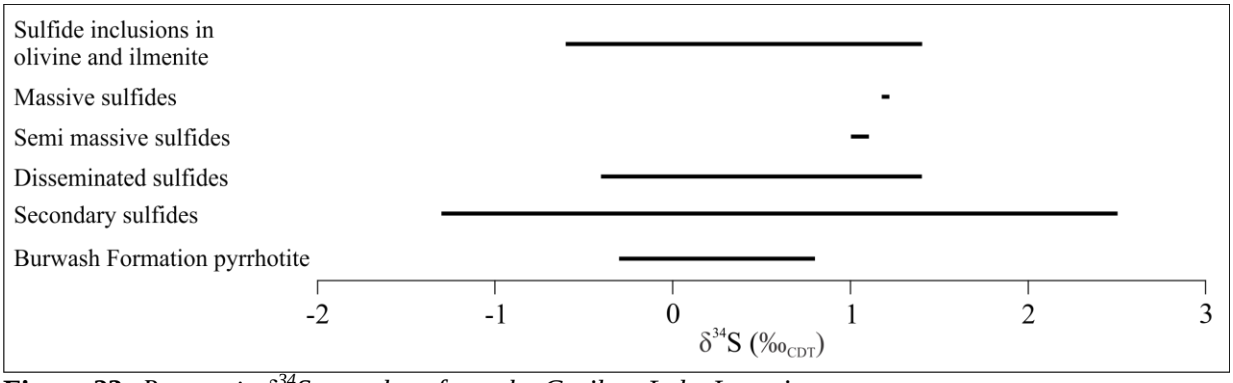

Figure 23: *Ranges in* $\delta^{34}S_{CDT}$ *values from the Caribou Lake Intrusion.*

Table 2: *Summary of $\delta^{34}S_{CDT}$ of primary and secondary sulfides*

Sample	δ^{34}S (‰CDT)	Sulfide	Sulfide Style	Generation
CL-06-16-47.6	1.2 ± 0.2	Po	Disseminated	Primary
CL-06-16-47.6	0.8 ± 0.2	Py	Fracture	Secondary
CL-06-16-52.5	1.2 ± 0.2	Po	Disseminated	Primary
CL-06-16-55.0	1.2 ± 0.2	Po	Disseminated	Primary
CL-06-16-56.3	1.3 ± 0.2	Po	Disseminated	Primary
CL-06-16-57.5	1.3 ± 0.2	Po	Disseminated	Primary
CL-06-16-58.6	1 ± 0.2	Po	Disseminated	Primary
CL-06-16-59.9	0.6 ± 0.2	Py	Fracture	Secondary
CL-06-16-61.7	1.2 ± 0.2	Po	Disseminated	Primary
CL-06-16-63.8	1 ± 0.2	Po	Disseminated	Primary
CL-06-16-78.75	1.2 ± 0.2	Po	Massive	Primary
CL-06-16-84.6	1.2 ± 0.2	Po	Massive	Primary
CL-06-01-22	1.1 ± 0.2	Po	Semi-Massive	Primary
CL-06-01-22.5	1.4 ± 0.2	Po	Disseminated	Primary
CL-06-05-77.72	2.5 ± 0.2	Po	Stringer	Secondary
CL-06-01-81.2	1.1 ± 0.2	Po	Massive	Primary
CL-06-05-81.6	1.3 ± 0.2	Po	Massive	Primary
CL-06-05-81.6	1 ± 0.2	Ccp	Semi-Massive	Primary
CL-07-01-115	0.0 ± 0.2	Po	Interstitial	Primary
CL-07-01-373	0.9 ± 0.2	Po	Interstitial	Primary
CL-07-01-422.9	0.9 ± 0.2	Po	Interstitial	Primary
CL-07-05-14	-0.4 ± 0.2	Po	Interstitial	Primary
CL-07-05-50	0.2 ± 0.2	Po	Interstitial	Primary
CL-07-14-323.5	0.3 ± 0.2	Po	Interstitial	Primary
C-L07-14-477.5	-0.1 ± 0.2	Po	Interstitial	Primary
CL-07-01-373-1	1.4 ± 0.2	Po	Interstitial	Primary
CL-07-01-373-2	0.7 ± 0.2	Po	Interstitial	Primary
CL-07-01-373-3	0.6 ± 0.2	Po	Interstitial	Primary
CL-07-01-373-4	0.5 ± 0.2	Po	Interstitial	Primary
CL-07-01-373-5	0.5 ± 0.2	Po	Interstitial	Primary
CL-07-01-373-6	0.6 ± 0.2	Po	Interstitial	Primary
CL-07-01-373-7	1.2 ± 0.2	Po	Interstitial	Primary
CL-07-01-373-1	-0.3 ± 0.3	Po	Inclusion in ilmenite	Primary
CL-07-01-373-2	0.1 ± 0.3	Po	Inclusion in ilmenite	Primary
CL-07-01-373-3	0.2 ± 0.3	Po	Inclusion in ilmenite	Primary
CL-07-01-373-4	1.4 ± 0.3	Po	Inclusion in ilmenite	Primary
CL-07-01-373-5	-0.1 ± 0.3	Po	Inclusion in ilmenite	Primary
CL-07-01-373-6	-0.1 ± 0.3	Po	Inclusion in ilmenite	Primary
CL-07-01-373-7	0.3 ± 0.3	Po	Inclusion in ilmenite	Primary
CL-07-01-373-1	1.0 ± 0.3	Po	Inclusion in olivine	Primary
CL-07-01-373-2	0.4 ± 0.3	Po	Inclusion in olivine	Primary
CL-07-01-373-3	0.4 ± 0.3	Po	Inclusion in olivine	Primary
CL-07-01-373-4	0.0 ± 0.3	Po	Inclusion in olivine	Primary
CL-07-01-373-5	0.5 ± 0.3	Po	Inclusion in olivine	Primary
CL-07-01-373-6	0.1 ± 0.3	Po	Inclusion in olivine	Primary

Table 2 (con't): *Summary of $\delta^{34}S_{CDT}$ of primary and secondary sulfides*

Sample	δ^{34}S (‰CDT)	Sulfide	Sulfide Style	Generation
CL-07-01-373-7	0.3 ± 0.3	Po	Inclusion in olivine	Primary
CL-07-01-373-8	-0.6 ± 0.3	Po	Inclusion in olivine	Primary
CL-07-01-373-1	0.6 ± 0.3	Po	Associated with actinolite	Primary
CL-07-01-373-2	0.9 ± 0.3	Po	Associated with actinolite	Primary
CL-07-01-373-3	1.1 ± 0.3	Po	Associated with actinolite	Primary
CL-07-01-373-4	0.6 ± 0.3	Po	Associated with actinolite	Primary
CL-07-01-373-5	1.0 ± 0.3	Po	Associated with actinolite	Primary
CL-07-01-373-6	0.9 ± 0.3	Po	Associated with actinolite	Primary
CL-07-01-373-7	0.9 ± 0.3	Po	Associated with actinolite	Primary
CL-06-05-77.72-1	0.9 ± 0.3	Po	Stringer	Secondary
CL-06-05-77.72-2	0.5 ± 0.3	Po	Stringer	Secondary
CL-06-05-77.72-3	0.1 ± 0.3	Po	Stringer	Secondary
CL-06-05-77.72-4	-1.3 ± 0.3	Po	Stringer	Secondary
CL-06-05-77.72-5	0.8 ± 0.3	Po	Stringer	Secondary
CL-06-05-77.72-6	1.7 ± 0.3	Po	Stringer	Secondary
CL-06-05-77.72-7	1.2 ± 0.3	Po	Stringer	Secondary
CL-06-16-35-1	-0.3 ± 0.3	Po	Burwash Sediments	Host Rock
CL-06-16-35-2	-0.1 ± 0.3	Po	Burwash Sediments	Host Rock
CL-06-16-35-3	0.5 ± 0.3	Po	Burwash Sediments	Host Rock
CL-06-16-35-4	-0.1 ± 0.3	Po	Burwash Sediments	Host Rock
CL-06-16-35-5	0.7 ± 0.3	Po	Burwash Sediments	Host Rock
CL-06-16-35-6	0.2 ± 0.3	Po	Burwash Sediments	Host Rock
CL-06-16-35-7	0 ± 0.3	Po	Burwash Sediments	Host Rock
CL-06-16-35-8	0.3 ± 0.3	Po	Burwash Sediments	Host Rock
CL-06-16-35-9	0.4 ± 0.3	Po	Burwash Sediments	Host Rock
CL-06-16-35-10	0.8 ± 0.3	Po	Burwash Sediments	Host Rock

Fluid Inclusion Petrography and Host Minerals

Apatite and Quartz Host Minerals

Apatite grains that will be studied for fluid inclusion analysis are hosted in moderately to highly altered mafic rocks. Petrography of inclusions has been conducted on four different samples, three gabbroic pegmatites and a diorite; microthermometry has yet to be performed. Alteration is extensive in numerous samples making it difficult to discern between clinopyroxene and orthopyroxene. In some instances primary mineralogy is completely altered, but relict textures in hand sample make it possible to identify the host lithologies as pegmatitic gabbros. Within the pegmatitic gabbro, apatite ranges in size from 0.2-12 mm (average 6 mm), euhedral-subhedral, and have tabular and irregular grain forms. Apatite occurs between clinopyroxene grains which have been subjected to strong amphibole and biotite alteration. In samples where alteration is extremely strong and original mineralogy is not identifiable, apatite grains range in size from 0.2-6 mm (average 2 mm), euhedral-anhedral, and have a variety of grain forms (prismatic, irregular, hexagonal, tabular). Alteration in these samples consists of amphibole, biotite, chlorite, serpentine, and sericite. Plagioclase tends to be relatively well preserved in the extremely altered samples but is highly fractured and altered along the fractures.

Quartz is rare but where it is present, it occurs as an interstitial phase between plagioclase, amphibole, biotite, and/or ilmenite within a moderately altered coarse grained diorite. Grains are anhedral and range in size from 1-8mm.

Fluid Inclusion Descriptions

A wide variety of fluid inclusions occur within apatite and quartz: 1) H_2O-CO_2-NaCl, 2) CO_2-NaCl, 3) H_2O-CO_2, 4) Polyphase brines, 5) Halite, 6) Opaque, and 7) CO_2.

Type 1: H_2O-CO_2-NaCl

Elongated primary H_2O-CO_2-NaCl inclusions occur in apatite where they display negative crystal form. Inclusions contain an aqueous phase (L_{aq}), CO_2 vapor bubble of variable volume percentage from one inclusion to another (V_{CO_2}, ≤40 vol%), and a small halite crystal (≤10 vol%) (Figure 23A). No other inclusions occur in primary assemblages with the H_2O-CO_2-NaCl inclusions.

Secondary H_2O-CO_2-NaCl inclusions in quartz are rare and do not appear trails with any other inclusion type. Halite crystals in these inclusions compose a minor percentage of the volume of the inclusion (< 5 vol%) and the V_{CO_2} is also volumetrically small (< 5 vol%). Inclusions are typically tabular and it is difficult to observe the small halite daughter phase when present (Figure 24A).

Type 2: CO_2-NaCl

Secondary inclusions in trails contain a V_{CO_2} bubble and a large halite crystal (~70 vol%). Inclusions are roughly spherical in shape and occasionally display a negative crystal form (Figure 23C). Other secondary trails contain CO_2-NaCl inclusions coevally trapped with H_2O-CO_2 inclusions (Figure 23D). All CO_2-NaCl inclusions only occur in apatite. Type 2 inclusions are only observed in apatite.

Trails of H_2O-CO_2-NaCl inclusions also occur coevally with H_2O-CO_2 inclusions and are interpreted to be secondary in origin, representing secondary immiscible brine – CO_2 assemblages, similar to assemblages that occur in the Stillwater Complex (Hanley et al, 2008) and in the Duluth Complex (Gál et al, 2013) (Figure 23B).

Type 3: H_2O-CO_2

H_2O-CO_2 inclusions occur within secondary trails along with Type 1 and Type 2 inclusions, as secondary trails consisting of only Type 3 inclusions, and as secondary inclusions that occur in clusters (Figure 23B,D,E,J). Inclusions that occur in clusters tend to be larger (≤ 20 um) than inclusions that occur in secondary trails (≤ 12 um). The amount of V_{CO_2} in the inclusions, regardless of occurring in a trail or cluster, is relatively consistent between 50 and 70 vol%. Shapes of inclusions that occur in secondary trails are generally circular or oval and may display negative crystal form. Inclusions associated with clusters are irregular and slightly tabular in shape.

Within quartz, H_2O-CO_2 inclusions occur in secondary trails or in clusters. The volume of the V_{CO_2} is variable and ranges from 10-50%. However, within a given assemblage V_{CO_2} proportions are similar (Figure 24B,C). Inclusions are subspherical, irregular, spherical, or tabular in shape and may have a negative crystal form.

Type 4: Polyphase brines

Polyphase brine inclusions contain a large V_{CO_2} (~40 vol%) that are surrounded by a thin film of L_{CO_2}. Halite crystals are variable in size and volume within the inclusion (5-10 vol%) (Figure 23F,G). Occasionally other solid transparent and opaque phases are present in these inclusions but these compose only a small percentage of the inclusions ($\leq$ 5 vol%). Liquid aqueous phase composes the remainder of the inclusion volume. Inclusions containing an opaque daughter phase have volumetrically equal proportions of V_{CO_2}, halite, and opaque phases ($\leq$ 5 vol%) (Figure 23I). Opaque bearing inclusions tend to occur in secondary trails composed of the same inclusions. Type 4 inclusions are only observed in apatite.

Type 5: Halite

Solid halite inclusions occur in secondary trails with vapor-halite inclusions. Halite inclusions are irregular in shape (Figure 23J). Type 5 inclusions are only observed in apatite.

Type 6: Opaque

Solid, square magnetite inclusions are euhedral and occur in secondary trails with V_{CO_2} inclusions, with other magnetite inclusions, or are solitary (Figure 23K). Type 6 inclusions are only observed in apatite.

Type 7: CO_2

Inclusions consisting of only CO_2 occur within secondary trails with Type 6 inclusions (Figure 23). Type 7 inclusions are circular to oval in shape and are common in apatite. Within quartz, CO_2 inclusions are common as secondary trails consisting only of CO_2 inclusions or with H_2O CO_2 inclusions with a high volume percent of CO_2 (>90 vol%), (Figure 22D). Inclusions are irregular, oval, circular, or tabular in shape and often display negative crystal form.

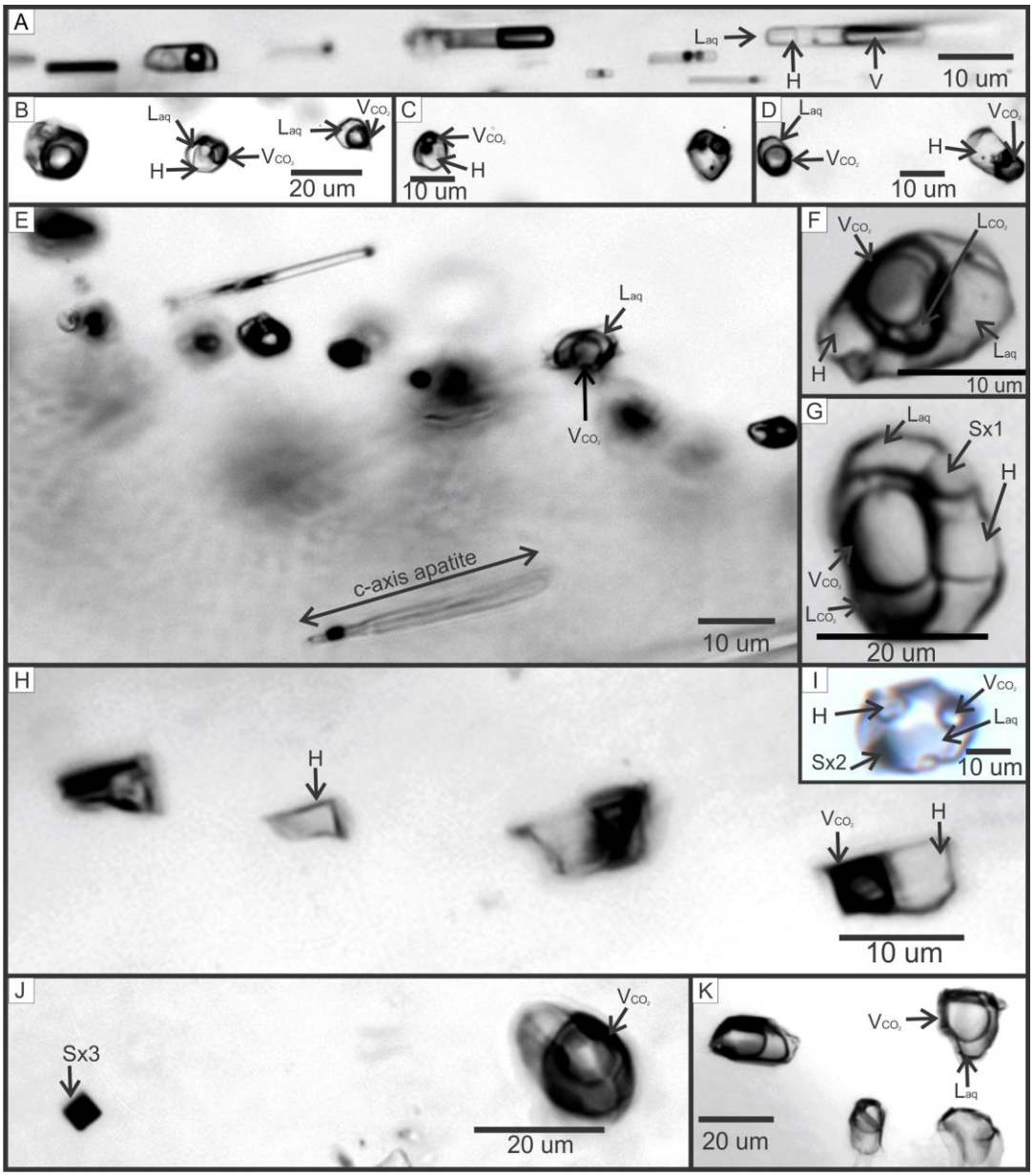

Figure 23: *Photomicrographs of fluid inclusions within apatite. A) Primary fluid inclusions (FI) that contain a halite crystal (H), vapour bubble (V), and an aqueous liquid phase (L_{aq}). These FI have an elongate shape, oriented parallel to the apatite host c-axis and show consistent liquid-vapor-halite ratios. B) Secondary FI trail containing two types of inclusions; 2 phase, L_{aq}-V_{CO2}- and 3 phase, L_{aq}-V_{CO2}-H-bearing inclusion. C) Secondary FI contain a large H crystal and a smaller CO_2 vapor phase. D) Secondary FI trail consisting of two types of inclusions. One type of inclusion has a large Vco_2 and a smaller L_{aq} phase. The other type of inclusion has a large H crystal and a smaller Vco_2. E) Secondary FI trail defined by 2-phase L_{aq}-V_{CO2} that contain a large vapor phase. Also present are primary FI oriented parallel to the c-axis of the apatite grain. F), G) and I) Secondary multiphase FI containing V_{CO2}-Lco_2-L_{aq}-H ± unidentified solid phase (Sx1) ± unidentified opaque solid phase (Sx2). H) Secondary FI trail containing H, V_{CO2} or H+V_{CO2} (V) and halite. J) Secondary inclusion trail containing an unknown (cubic?) opaque solid grain (Sx2) and a larger V_{CO2}-L_{CO2} inclusion. K) Secondary inclusions containing V_{CO2}–L_{CO2} and L_{aq}. All photomicrographs taken at 20°C.*

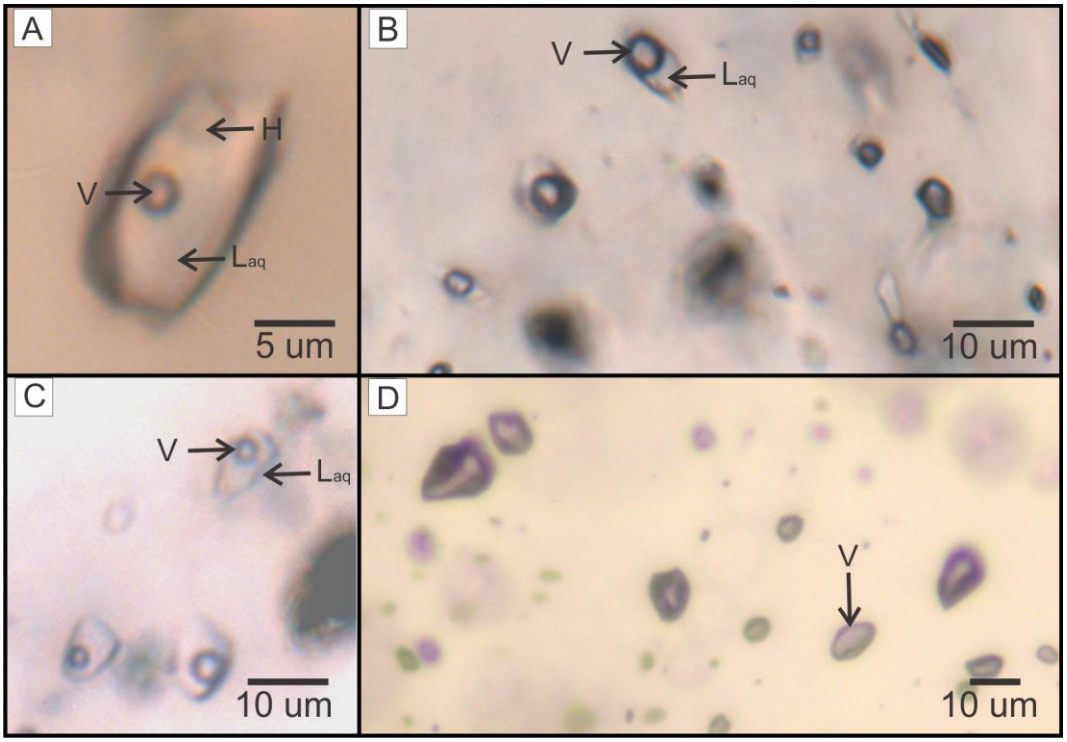

Figure 24: *Fluid inclusions within quartz. A) Secondary inclusion comprised of a small V and halite crystal. B) Secondary V-L_{aq} inclusion trail with relatively consistent V proportions (~40 vol%). C) Secondary V_{CO2}-Laq inclusion cluster with relatively consistent V proportions (~20 vol%). D) Secondary V inclusion trail.*

Preliminary Conclusions and Future Work

Initial petrography has shown that the CLI is composed primarily of various gabbroic and ultramafic units that can be enriched in olivine, Fe-Ti oxides, plagioclase, or clinopyroxene. Ultramafic sequences within the CLI vary between dunites and clinopyroxenites that are occasionally rich in Fe-Ti oxides and may be interrupted by short intervals of pegmatitic gabbros.

Chondrite-normalized plots of unaltered, altered fine grained gabbros, and pegmatites within the CLI display a negative slope, which is typical of a garnet lherzolite source. An outlier present in Figure 21A,B is a very coarse grained to pegmatitic gabbro rich in apatite, indicated by elevated P_2O_5 (0.85 wt%) compared to other units (≤0.42 wt% P_2O_5). The outlier is highly enriched in all REE compared to other pegmatites and exhibits a negative Eu anomaly rather than a positive anomaly. Trace element diagram of pegmatites (Figure 21B) shows the outlier is enriched in all trace elements (except Sr) and apatite would seem to be the main phase controlling the trace element distribution but zircon may be a trace phase present and control the HREE, indicated by Zr concentration in whole rock geochemistry is 1109 ppm. The high amounts of vanadium provide constraint on fO_2 in the system. Toplis and Corgne (2002) have demonstrated that with vanadium contents this high, the unit crystallized close to the Ni-Ni-O buffer (between Ni-Ni-O and Ni-Ni-O -1.5). Combined with the ilmenite exsolution textures in magnetite, fO_2 of the system will be well constrained in the intrusion.

Investigation of the mineralized intervals within the CLI has revealed a simple sulfide mineral assemblage. Sulfide mineralogy is dominated by pyrrhotite, with lesser amounts of chalcopyrite, pyrite, pentlandite, and sphalerite. Pentlandite most commonly occurs as discrete grains or in chains within pyrrhotite and has a tendency to concentrate near chalcopyrite. Flame lamellas of pentlandite are present but less common. Trace metal minerals within mineralized zones include galena, glaucodot-gersdorffite, molybdenite, nickeline, melonite, electrum, and unidentified Se-Te-Pb, Bi-Te, and Pb-Te minerals that occur as inclusions within gersdorffite. These trace metals minerals, except for galena, are concentrated along grain boundaries of pyrrhotite or along quartz in-filled fractures which would indicate they are likely related to a secondary mineralized fluid rather than being primary magmatic in origin.

Sulfur isotope compositions, regardless of being primary or secondary in origin, or related to the host rocks of the intrusion, are consistent with a mantle source of 0 ± 2 ‰ (Ohmoto and Rye, 1979). However, with the $\delta^{34}S$ values of sulfur from the Burwash Formation being within the mantle source range, it is not possible to tell from sulfur isotopes the relative role of contamination the Burwash Formation would have had on the intrusion.

Fluid inclusions are extremely well preserved within the CLI, and are primarily hosted by large (~6 mm) apatite grains within pegmatitic gabbros. Quartz also hosts inclusions but the amount of quartz present within the intrusion compared to apatite is minimal. Primary H_2O-CO_2-NaCl inclusions occur in apatite, elongated parallel to the c-axis. A variety of secondary inclusions are present and consist of: 1) immiscible brine – CO_2, 2) halite, 3) opaque, 4) polyphase brines, and, 5) vapor-rich (>90 vol% vapour) inclusions. Fluid inclusions occurring in quartz are secondary and vapour-rich with minor H_2O-CO_2-NaCl and vapour-poor (<15vol% vapour) inclusions Inclusions present are similar to inclusions that have been observed at the Stillwater Complex (Hanley et al, 2008), Duluth Complex, (Gál et al, 2013), and Lac des Iles (Hanley and Gladney, 2011). Lac des Iles contains abundant primary CO_2 inclusions and LA-ICPMS has shown that these inclusions can carry Ni, Cu, Pd, Bi, Te, and Fe, which suggest the carbonic fluids have played a role in the precipitation and mobilization of metals in the system (Hanley and Gladney, 2011). With abundant secondary CO_2 inclusions present within the CLI it is possible that a secondary carbonic fluid may have remobilized metals. This will be verified by LA-ICPMS analysis of individual inclusions. Microthermometry of fluid inclusions will be carried out in order to evaluate the temperature and depth of the intrusion and determine which types of fluids were involved in metal remobilization and alteration of the system.

Acknowledgements

The authors would like to thank numerous people and organizations for their support through the first year of this project. In particular, we would like to thank the Northwest Territories Geoscience Office, Aurora Geoscience, and the staff at Blachford Lake Lodge for providing financial, logistical, and technical support. Also, we would like to thank Scott Cairns and Shevaun McGoldrick for their capable and enthusiastic field assistance, and to John Ketchum allowing for a chance to see the Thor Lake REE deposit and the wide range of rocks that compose the Blatchford Lake intrusive suite. Finally the authors would like to recognized Gold Fields Exploration Inc and the Society for Economic Geologist for their generous scholarship and NSERC-DG to Dr. Hanley for student support.

References

Birkett, T.C., Richardson, D.G. and Sinclair, W.D., 1994. Gravity modeling of the Blachford Lake Intrusive Suite, Northwest Territories. *In* Studies of rare-metal deposits in the Northwest Territories. *Edited by* W.D. Sinclair and D.G. Richardson. Geological Survey of Canada, p. 5-16.

Bowring, S. A., Van Schmus, W. R. & Hoffman, P. F., 1984. U-Pb zircon ages from Authapascow Aulacogen, East Arm of Great Slave Lake, NWT, Canada. Canadian Journal of Earth Sciences, v. 21, p. 1315-1324.

Crowe, D.E. and Vaughn, R.G., 1996. Characterization and use of isotopically homogeneous standards for in situ laser microprobe analysis of $^{34}S/^{32}S$ ratios. American Mineralogist, v. 81, p. 187-193.

Davidson, A., 1972. Granite Studies in the Slave Province. *Report of Activities*: Geological Survey of Canada, p. 109-115.

Davidson, A., 1978. The Blachford Lake Intrusive Suite: An Aphebian alkaline plutonic complex in the Slave Province, Northwest Territories. *Current Research*: Geological Survey of Canada, p. 119-127.

Davidson, A., 1981. Petrochemistry of the Blachford Lake Complex, District of Mackenzie. *Geological Survey of Canada Open File 764*, 24 p.

Davidson, A., 1982. Petrochemistry of the Blachford Lake complex near Yellowknife, Northwest Territories. In: Maurice, Y. T. (ed.) *Uranium in Granites*: Geological Survey of Canada, 71-79.

Curry, J.D., Lee, W.K., and Overveld, R., 1963. Earl-Jack Syndicate exploration report; submitted by Earl Jack Syndicate, Department if Indian and Northern Affairs, Activities Report 015065, 2 p.

Curry, J.D., 1969. Electromagnetic and magnetic geophysical surveys for parts of the NC claim group; submitted by Shield Resources Ltd, Department of Indian Affairs and Northern Development, Activities Report 018838, 6 p.

Gál, B., Molnár, F., Guzmics, T., Mogessie, A., Szabó, C., and Peterson, D., 2013. Segregation of magmatic fluids and their potential in the mobilization of platinum group elements in the South Kawishiwi Intrusion, Duluth Complex, Minnesota – Evidence from petrography, apatite geochemistry, and coexisting fluid and melt inclusions. Ore Geology Reviews, v. 54, p. 59-80.

Hanley, J.J., Mungall, J.E., Pettke, T., Spooner, E.T.C., and Bray, C.J., 2008. Fluid and Halide Melt Inclusions of Magmatic Origin in the Ultramafic and Lower Banded series, Stillwater Complex, Montana, USA. Journal of Petrology, v. 49, p. 1133-1160.

Hanley, J.J., and Gladney, E.R., 2011. The presence of carbonic-dominated volatiles during the crystallization of sulfide-bearing mafic pegmatites in the North Roby Zone, Lac des Iles Complex, Ontario. Economic Geology, v. 106, p.33-54.

Hoffman, P.F., 1980. Wopmay Orogen: a Wilson cycle of early Proterozoic age in 99 the Northwest of the Canadian Sheild. *In* The continental crust and its mineral deposits. *Edited by* D.W. Strangway. Geological Association of Canada, Special Paper 20, p. 523-549.

Irvine, T.N., and Baragar, W.R.A., 1971. A guide to the chemical classification of the common volcanic rocks: Canadian Journal of Earth Sciences, v. 8, p. 523-548.

Jensen M. L. and Nakai N., 1962. Sulfur isotope meteorite standards, results and recommendations. In *Biogeochemistry of Sulfur Isotopes*, NSF Symposium, p. 30-35.

Ludington, S., 1978, The biotite-apatite geothermometer revisted. American Mineralogist, v. 63, p. 551-553.

Marmont, C., 2006. Report on Diamond Drilling, Airborne and Ground Geophysical Surveys, Lithogeochemical Sampling and Prospecting; submitted by Kodiak Exploration, Northwest Territories Geoscience Office, Activities Report 085101, p. 123.

Marmont, C., 2007. Report on diamond drilling; submitted by Kodiak Exploration, Northwest Territories Geoscience Office, Activities Report 085317, p. 283.

Mumford, T., 2013. Petrology of the Blatchford Lake Intrusive Suite, Northwest Territories Canada. *Unpublished* Ph.D. thesis, Carleton University. 240 p.

Ohmoto, H., and Rye, R.O., 1979. Isotopes of sulfur and carbon, *in* Barnes, H.L., ed., Geochemistry of hydrothermal ore deposits, 2nd ed.: New York, Wiley, p. 509-567.

Pilkington, M., Thomas, M.D, and Mumford, T.R., 2012. Geological significance of a new high resolution gravity gradiometric and magnetic survey over the Blatchford Lake Complex, Northwest Territories; Geological Survey of Canada, Open File 7084, Poster.

Riciputi, L.R., Paterson, B.A. and Ripperdan, R.L., 1998. Measurement of light stable isotope ratios by SIMS: Matrix effects for oxygen, carbon, and sulfur isotopes in minerals. International Journal of Mass Spectrometry, v. 178, p. 81-112.

Ripley, R., 1990. Se/S ratios od the Virginia Formation and Cu-Ni sulfide mineralization in the Babbitt area, Duluth Complex, Minnesota. Economic Geology, v. 85, p. 1935-1940.

Ripley, E.M., and Li, C. (2003): Sulfur isotope exchange and metal enrichment in the formation of magmatic Cu-Ni-(PGE) deposits. Economic Geology, v. 98, p. 635-641.

Sinclair, W. D., Hunt, P. A. & Birkett, T. C., 1994. U-Pb zircon and monazite ages of the Grace Lake Granite, Blatchford Lake Intrusive Suite, Slave Province, Northwest Territories. *Radiogenic Age and Isotopic Studies: Report 8; Geological Survey of Canada, Current Research 1994-F*, 15-20.

Sun, S., and McDonough, W.F., 1989. Chemical and isotopic systematics of oceanic basalts: implications for mantle composition and processes. In Saunders, A.D., and Norry, M.J., (eds.) Magmatism in the Ocean Basins. Geological Society Special Publication No. 42, p. 313-345.

Toplis, M.J., and Corgne, A., 2002. An experimental study of element partitioning between magnetite, clinopyroxene, and iron-bearing silicate liquids with particular emphasis on vanadium. Contributions to Mineralogy and Petrology, v. 144, p. 22-37.

Wanless, R. K., Stevens, R. D., Lachance, G. R. & Delabio, R. N., 1979. District of Mackenzie. In: Geological Survey of Canada - Radiogenic age and isotopic studies, R. (ed.), p. 34-38.

Warman, T.A, and Gelo, K.K., 1995. Assessment report on the geological and geophysical programs conducted of the Bagpipe claims, Mackenzie Mining District, Northwest Territories; submitted by Caledonia Mining Corporation, Department of Indian and Northern Affairs, Activities Report 083658, 122 p.

Appendix A: *February 2013 Sample List*

Sample	Description
CL-07-01-8	Very coarse grained leucogabbro
CL-07-01-115.7	Very coarse grained gabbro, 1% Po
CL-07-01-167.76	Pegmatoidal gabbro, shows signs of fluid interactment
CL-07-01-322.4	Fine-medium grained gabbro, 1% Po, magnetite rich
CL-07-01-325.6	Fine grained gabbro
CL-07-01-354.2	Medium grained gabbro
CL-07-01-371.2	Medium grained gabbro, Tr Po, 10% Mag
CL-07-01-373	Coarse grained gabbro, shows signs of serpentinization, Tr Po
CL-07-01-380	Coarse grained gabbro, shows signs of serpentinization, Tr Po
CL-07-01-422.9	Fine grained gabbro, 1% Po, mangetite rich
CL-07-02-347	Medium grained gabbro, highly serpentinized?
CL-07-03-169	Fine-medium grained gabbro
CL-07-05-11	Medium grained gabbro, pyroxene rich
CL-07-05-14	Coarse grained gabbro, Tr Po blebs
CL-07-05-30.2	Coarse grained gabbro
CL-07-05-50	Very coarse grained gabbro, 10-15% 1-2cm blebs of Po, Cp concentrated around Po grains
CL-07-05-105	Very coarse grained leucogabbro
CL-07-07-117	Magnetite rich ultramafic rock, 1% Po
CL-07-05-142.5	Gabbro, 1% Po
CL-07-05-144	Magnetite rich ultramafic rock (pyroxenite?), 1% Po
CL-07-05-499	Very coarse grained gabbro, < 1% Po
CL-07-05-675	Magnetite rich ultramafic, Mag crystals look like a cumulate texture in areas
CL-07-07-10.1	Medium grained leucogabbro, Tr Po
CL-07-07-17	Medium-coarse grained leucogabbro, Tr Po
CL-07-07-450	Coarse grained gabbro
CL-07-07-483	Very coasre grained leucogabbro, Tr Po
CL-07-14-323.5	Very coarse grained gabbro
CL-07-14-477.4	Coarse grained gabbro, 5-10% Po, Cp concentrated on rims of Po
CL-07-15-145	Extemely coarse grained norite

Appendix B: *Summer 2013 Sample List*

Sample	Description
CL-06-16-8.9	Gabbro. Grains ≤4mm. Trace pyrrhotite. 5-10% < 2mm interstitial magnetite.
CL-06-16-11.2	Gabbro. Grains ≤4mm. Trace pyrrhotite. 5-10% < 4mm interstitial magnetite.
CL-06-16-14.1	Syenite vein crosscutting gabbroic units
CL-06-16-33.7	Gabbro. Grains <2mm. Trace pyrrhotite. 5% interstitial magnetite
CL-06-16-35.7	Pyroxenite. Grains <12mm. 2% pyrrhotite. 10-15% <6mm interstitial magnetite
CL-06-16-47.0	Gabbro. Grains <3mm. 5% pyrrhotite. 5% < 3mm interstitial magnetite.
CL-06-16-47.6	Gabbro. Grains <3mm. 25% pyrrhotite. 5% < 3mm interstitial magnetite.
CL-06-16-51.2	Syenite vein crosscutting gabbroic units
CL-06-16-52.5	Gabbro with highly disseminated pyrrhotite (20-30%). Grains ≤5mm. 10% interstitial magnetite.
CL-06-16-55.0	Gabbro with highly disseminated pyrrhotite (20-30%). Grains ≤5mm. 10% interstitial magnetite.
CL-06-16-56.3	Gabbro with highly disseminated pyrrhotite (20-30%). Grains ≤5mm. 10% interstitial magnetite.
CL-06-16-57.5	Gabbro with highly disseminated pyrrhotite (20-30%). Grains ≤5mm. 10% interstitial magnetite.
CL-06-16-58.6	Gabbro with highly disseminated pyrrhotite (20-30%). Grains ≤5mm. 10% interstitial magnetite.
CL-06-16-59.9	Gabbro. Grains <2mm. 2% pyrrhotite. 5-10% interstitial <2mm magnetite.
CL-06-16-61.7	Gabbro with highly disseminated pyrrhotite (20-30%). Grains ≤5mm. 10% interstitial magnetite.
CL-06-16-63.15	Gabbro, Grains <3mm. Trace pyrrhotite. 5% <2mm interstitial magnetite
CL-06-16-63.8	Gabbro. Grains <15mm. Trace pyrrhotite. 5%, <5mm interstitial magnetite
CL-06-16-65.7	Quartz syenite vein crosscutting gabbro
CL-06-16-71.15	Gabbro. Grains <3mm. 5-10% pyrrhotite. 5%, <2mm interstitial magnetite
CL-06-16-78.75	Gabbro. Grains <15mm. Trace pyrrhotite. 5% <4mm interstitial magnetite
CL-06-16-80.0	Gabbro. Grains <15mm. Trace pyrrhotite. 5% <4mm interstitial magnetite
CL-06-16-83.5	Gabbro. Grains <2mm. Trace pyrrhotite. 5% interstitial magnetite
CL-06-16-84.6	Massive pyrrhotite
CL-06-16-90.0	Gabbro. Grains <3mm. Trace pyrrhotite. 5%, <2mm interstitial magnetite, locally rich in plagioclase
CL-06-16-103.0	Altered gabbro, bleaching and abundant epidote and chlorite stringers throughout
CL-06-16-152.45	Gabbro. Grains <1mm. Trace pyrrhotite. 5% interstitial magnetite
CL-06-16-155.6	Quartz syenite vein crosscutting gabbro
CL-06-16-170.6	Carbonate altered diabase
CL-06-39-4.1	Pegmatitic gabbro. Grains <60mm. 10% 5-20mm interstitial magnetite
CL-06-39-6.85	Pegmatitic gabbro. Plagioclase, 30%, 5-25mm. Pyroxene, 60%, 10-60mm. Magnetite, 10%, 7-12mm.
CL-06-39-10.98	Gabbro, coarse grained. Plagioclase , 30-40%, 3-7mm. Pyroxene, 40%, 4-7mm. Magnetite, interstitial, 20%, 3-6mm.
CL-06-39-17.2	Gabbro. Grains ≤3mm. Trace pyrrhotite. 5-10% < 4mm interstitial magnetite.
CL-06-39-20.35	Ultramafic. <5%, 1-3mm Plag. Highly serpentinized, formerly dunite?

Sample	Description
CL-06-39-32.21	Feldspathic ultramafic. 10% plagioclase, <4mm. 20% interstitial magnetite, <8mm. Highly serpentinized, formerly dunite?
CL-06-39-32.82	Ultramafic. 5% plagioclase, <4mm. 20% interstitial magnetite, <8mm. Highly serpentinized, formerly dunite?
CL-06-39-33.28	Ultramafic. Trace plagioclase, <4mm. 15% interstitial magnetite, <8mm. Highly serpentinized, formerly dunite?
CL-06-39-47.36	Pegmatitic gabbro. Plagioclase, >15mm, 60%. Pyroxene, <25mm, 30%. Biotite, 5mm, 2-4%.
CL-06-39-57.38	Gabbro. Grains ≤3mm. Trace pyrrhotite. 5-10% < 4mm interstitial magnetite.
CL-06-39-60.23	Feldspathic ultramafic. 15-20% plagioclase, <5mm. 20% interstitial magnetite, <7mm. Highly serpentinized, formerly dunite?
CL-06-39-63.88	Feldspathic ultramafic. 15-20% plagioclase, <5mm. 20% interstitial magnetite, <7mm. Highly serpentinized, formerly dunite?
CL-06-39-83.9	Highly altered ultramafic. Olivine grains altered to a cream colour (?)
CL-06-39-94.95	Feldspathic ultramafic. 15-20% plagioclase, <5mm. 20% interstitial magnetite, <7mm. Highly serpentinized, formerly dunite?
CL-06-39-100.0	Pegmatitic anorthosite. Plagioclase, >30mm, 90%. Magnetite, 6-12mm, 5%. Biotite, 10mm, 2-3%.
CL-06-39-103.55	Gabbro. Grains <8mm. Magnetite, interstitial, 10%, <8mm.
CL-06-39-103.7	Feldspathic ultramafic. 15-20% plagioclase, 3-10mm. 10% interstitial magnetite, <5mm.
CL-06-39-103.91	Pegmatitic anorthosite. Plagioclase, >30mm, 90%. Magnetite, 6-12mm, 5%. Biotite, 10mm, 2-3%.
CL-06-39-105.83	Gabbro. Grains <5mm. Magnetite, interstitial, 15%, <3mm.
CL-06-39-108.0	Feldspathic ultramafic. 15-20% plagioclase, 3-10mm. 10% interstitial magnetite, <5mm.
CL-06-39-118.75	Gabbro. Grains 5-12mm. Magnetite, interstitial, 10%.
CL-06-39-122.3	Diorite. Pyroxene, 5-10%, interstitial, 2-5mm. Magnetite, interstitial, <3mm, 2%.
CL-06-39-125.0	Anorthosite. Grains 3-15mm.
CL-06-39-128.4	Gabbro. Grains <4mm. Magnetite, interstitial, 10%.
CL-06-39-132.47	Pegmatitic Gabbro. Plagioclase, 6-20mm, 40%. Pyroxene, 8-80mm, 40%. Magnetite, 4-15mm, 10%.
CL-06-39-133.4	Pegmatitic Gabbro. Plagioclase, 6-20mm, 40%. Pyroxene, 8-80mm, 40%. Magnetite, 4-15mm, 10%.
CL-06-39-150.08	Gabbro. Grains <8mm. Magnetite, interstitial, <4mm, 5-10%.
CL-06-39-154.16	Feldspathic ultramafic. Plagioclase 10-15%, 2-6mm. Magnetite, 20%, 2-5mm.
CL-06-39-156.97	Pegmatitic gabbro. Plagioclase and pyroxene, up to 5cm. Magnetite, interstitial, 5%, <5mm.
CL-07-01-9.1	Pegmatitic gabbro. Graphic texture between pyroxene and magnetite. Subophitic textures.
CL-07-01-29.1	Gabbro. Grains < 12mm. Plagioclase is altered to a cream colour rather than being white like in other units.
CL-07-01-50.2	Feldspathic ultramafic. Plagioclase, 10-15%, 1-4mm. Ophitic textures.
CL-07-01-52.3	Gabbro. Grains < 12mm. Magnetite, 2-10mm, 10-15%. Trace amounts of interstitial quartz.
CL-07-01-55.9	Gabbro. Grains < 12mm. Magnetite, 2-10mm, 10-15%. Trace amounts of interstitial quartz.
CL-07-01-67.5	Pegmatitic gabbro. Plagioclase and pyroxene, up to 5cm. Magnetite, interstitial, 20%, 2-20mm.
CL-07-01-76.9	Pegmatitic gabbro. Plagioclase and pyroxene, up to 5cm. Magnetite, interstitial, 20%, 2-20mm.
CL-07-01-79.3	Gabbro. Plagioclase and pyroxene 3-12mm. Magnetite, 2-10mm, 10-15%. 2% biotite, associated with magnetite. 2% pyrrhotite
CL-07-01-95.9	Pegmatitic gabbro. Plagioclase and pyroxene, up to 5cm. Magnetite, interstitial, 20%, 2-20mm.

Sample	Description
CL-07-01-101	Plagioclase rich gabbro. Plagioclase, 50-60%, 3-12mm. Pyroxene, 30-35%, 2-8mm.
CL-07-01-113.8	Plagioclase rich gabbro. Plagioclase, 50-60%, 3-12mm. Pyroxene, 30-35%, 2-8mm. Trace amounts of pyrrhotite and biotite.
CL-07-01-117.2	Pyroxenite. Grains <10mm. Magnetite, 1-5mm, 20%, interstitial.
CL-07-01-124.3	Gabbro. Grains <4mm. Magnetite, interstitial, 20%.
CL-07-01-127	Pegmatitic gabbro. Plagioclase and pyroxene <70mm. Magnetite, 2-25mm, 10%. Trace apatite?
CL-07-01-128.1	Gabbro. Grains <10mm. Magnetite, interstitial, 10-20%.
CL-07-01-134.3	Pegmatitic gabbro. Plagioclase and pyroxene 10-50mm. Magnetite, 2-20mm, 20%. Trace biotite.
CL-07-01-140	Gabbro. Grains <4mm. Magnetite, interstitial, 25-30%.
CL-07-01-145.7	Pegmatitic gabbro. Plagioclase and pyroxene 10-50mm. Magnetite, 2-20mm, 20%. Trace biotite.
CL-07-01-156.3	Pegmatitic gabbro. Plagioclase and pyroxene 10-50mm. Magnetite, 2-20mm, 20%. Trace biotite.
CL-07-01-166.4	Gabbro. Grains <10mm. Magnetite, interstitial, 10-20%.
CL-07-01-171.5	Pegmatitic gabbro. Plagioclase and pyroxene 10-50mm. Magnetite, 2-20mm, 20%. Trace biotite.
CL-07-01-173.9	Pegmatitic gabbro. Plagioclase and pyroxene 10-50mm. Magnetite, 2-20mm, 20%. Trace biotite.
CL-07-01-180.1	Pegmatitic gabbro. Plagioclase and pyroxene 10-50mm. Magnetite, 2-20mm, 20%. Trace biotite.
CL-07-01-203.6	Gabbro. Grains <10mm. Magnetite, interstitial, 10-20%.
CL-07-01-222.1	Pegmatitic gabbro. Plagioclase and pyroxene 10-50mm. Magnetite, 2-20mm, 20%. Trace biotite.
CL-07-01-233	Silicified gabbro?
CL-07-01-249.9	Gabbro. Grains <8mm. Magnetite, 1-4mm, interstitial, 5-10%. Trace biotite.
CL-07-01-251.6	Granitic vein crosscutting gabbros. "sugary" appearance.
CL-07-01-271	Gabbro. Grains 3-15mm. Magnetite, 1-10mm, 15-20%.
CL-07-01-275.7	Pegmatitic gabbro. Plagioclase and pyroxene 10-50mm. Magnetite, 2-20mm, 20%. Trace biotite.
CL-07-01-277.4	Gabbro. Grains <8mm. Magnetite, 1-4mm, interstitial, 5-10%. Trace biotite. Trace quartz.
CL-07-01-287.1	Gabbro. Grains <8mm. Magnetite, 1-6mm, interstitial, 15%.
CL-07-01-308.8	Gabbro. Grains <8mm. Magnetite, 1-6mm, interstitial, 15%. Magnetite also occurs as bands across the sample.
CL-07-01-327.3	Gabbro. Grains <3mm. Magnetite, 10-15%.
CL-07-01-329	Magnetitite. 50-70% Magnetite, 1-6mm, forming a net texture.
CL-07-01-367	Magnetitite. 50-70% Magnetite, 1-6mm, forming a net texture.
CL-07-01-381.7	Pegmatitic gabbro. Plagioclase and pyroxene 8-35mm. Magnetite, 8-20mm, 10-15%. Trace biotite.
CL-07-01-411.6	Gabbro. Grains <20mm. Magnetite, 1-10mm, 15%. Trace apatite.
CL-07-01-429.8	Granitic package at bottom of hole. Quartz syenite.
CL-07-11-494.6	Morose granite. Weakly foliated. Locally megacrystic
CL-07-14-107.8	Whiteman Lake quartz syenite
CL-07-14-208.9	Whiteman Lake quartz syenite

Sample	Description
CL-06-44-58.8	Leucoferrodiorite
CL-06-50-150	Hearne granite
GLG	Grace Lake granite
CL-06-35-56.36	Burwash sediments
CL-06-01-18.8	5-10% disseminated pyrrhotite. Hosted in 2-8mm gabbro.
CL-06-01-22.0	10-15% disseminated pyrrhotite. Pyrrhotite has been partial replaced by pyrite, 10-15%. 2% chalcopyrite. Hosted in 5-15mm gabbro.
CL-06-01-22.5	20-25% disseminated pyrrhotite. 2% chalcopyrite. Hosted in 5-15mm gabbro.
CL-06-05-75.1	10-15% disseminated pyrrhotite, <2mm. Hosted in <3mm gabbro.
CL-06-05-77.72	10-15% disseminated pyrrhotite, <2mm. Hosted in <3mm gabbro. 3mm band of chalcopyrite and pyrrhotite crosscutting gabbro.
CL-06-05-81.2	Massive Pyrrhotite. Magnetite, 10%,1-4mm. Chalcopyrite, 2%,<2mm.
CL-06-05-81.6	Massive Pyrrhotite. Magnetite, 10%,1-4mm. Chalcopyrite, 2%,<2mm. Two bands of Chalcopyrite present.
CL-07-09-57	Fine grained gabbro. Assay results from Kodiak indicate 118.4 ppb Pt + Pd
CL-07-09-60	Fine grained gabbro. Assay results from Kodiak indicate 214.1 ppb Pt + Pd

Appendix C: *Whole rock geochemistry of February 2013 sample set.*

Drill Hole	CL-07-01	CL-07-01	CL-07-01	CL-07-01	CL-07-01	CL-07-01	CL-07-01	CL-07-01	CL-07-01
Depth (m)	8	115.7	167.76	322.4	325.6	354.2	371.2	373	380
SiO_2(wt%)	46.53	42.62	39.14	21.87	43.69	41.30	41.88	35.96	39.07
TiO_2	2.60	2.25	2.61	>8.00	2.70	3.25	3.65	6.42	4.01
Al_2O_3	18.34	15.88	13.30	8.80	11.07	12.45	12.99	11.84	16.68
Fe_2O_3	11.28	13.08	18.38	44.75	15.96	19.95	18.97	29.09	19.53
MnO	0.24	0.14	0.19	0.33	0.20	0.22	0.22	0.29	0.22
MgO	3.73	8.10	8.31	4.16	8.62	7.97	7.23	8.10	5.91
CaO	7.28	13.01	10.17	6.03	13.75	10.46	10.88	5.15	7.49
Na_2O	3.88	1.71	1.86	1.15	1.73	2.16	2.26	2.03	2.60
K_2O	1.69	0.53	0.44	0.20	0.15	0.24	0.27	0.65	0.68
P_2O_5	0.25	0.06	0.35	0.09	0.04	0.17	0.12	0.11	0.12
L.O.I.	3.30	1.40	4.15	-0.49	0.81	0.48	0.59	-0.08	2.42
Total	99.13	98.78	98.90	99.30	98.72	98.65	99.06	99.56	98.73
Ba (ppm)	524.30	144.70	199.30	85.20	99.30	150.60	148.90	166.90	193.00
Be	0.61	0.37	0.57	0.28	0.42	0.54	0.49	0.63	0.79
Bi	<0.15	0.15	<0.15	<0.15	<0.15	<0.15	<0.15	<0.15	<0.15
Cd	0.17	0.20	0.21	0.13	0.15	0.12	0.14	0.09	0.42
Ce	20.13	11.33	31.81	10.37	12.68	20.12	15.46	13.73	13.21
Co	21.98	65.66	59.53	137.83	65.30	88.04	72.80	104.46	73.21
Cr	17.00	660.00	71.00	105.00	486.00	321.00	163.00	57.00	17.00
Cs	1.77	0.38	2.00	0.20	0.26	0.26	0.36	1.03	4.60
Cu	2.00	363.90	142.40	92.80	92.10	197.20	65.70	54.50	18.60
Dy	1.74	1.38	3.03	1.14	2.27	2.21	1.81	1.10	0.77
Er	0.64	0.56	1.12	0.48	0.92	0.89	0.73	0.49	0.32
Eu	2.11	0.98	2.02	0.72	1.29	1.41	1.34	0.98	1.11
Ga	21.11	21.52	22.59	34.17	18.06	20.55	21.29	21.66	21.66
Gd	2.63	1.93	4.56	1.63	3.02	3.06	2.50	1.53	1.19
Hf	1.23	1.09	1.54	2.01	1.44	1.28	1.03	1.62	0.84
Ho	0.28	0.24	0.49	0.20	0.38	0.37	0.30	0.19	0.13
In	0.07	0.06	0.08	0.10	0.08	0.07	0.07	0.06	0.05
La	8.57	4.87	12.56	4.27	4.47	8.43	6.73	6.29	6.27
Li	24.90	13.60	18.90	11.20	10.10	8.50	14.70	17.30	31.10
Lu	0.06	0.05	0.10	0.05	0.09	0.09	0.07	0.06	0.03
Mo	1.38	1.32	0.73	1.52	0.69	0.83	0.73	1.18	0.75
Nb	9.53	3.86	9.10	22.36	3.96	7.05	6.31	17.81	7.75
Nd	13.41	7.98	22.30	7.04	10.88	13.73	10.73	7.97	7.22
Ni	4.80	489.70	190.20	125.70	139.60	179.70	88.50	40.80	20.20
Pb	4.00	1.60	1.80	1.40	0.80	1.00	0.90	2.30	13.30
Pr	2.90	1.69	4.72	1.51	2.14	2.92	2.27	1.85	1.73
Rb	55.97	8.30	13.27	4.19	2.68	3.48	3.81	22.65	25.98
Sb	<0.04	<0.04	<0.04	<0.04	<0.04	<0.04	<0.04	<0.04	0.04
Sc	10.80	26.30	13.20	18.90	40.90	26.10	25.50	8.80	4.60
Sm	2.95	1.98	5.05	1.70	2.98	3.25	2.61	1.73	1.40
Sn	10.97	0.69	1.51	0.90	0.45	0.52	0.43	0.95	5.27
Sr	1172.60	683.90	672.50	350.30	560.40	622.70	670.10	697.70	1054.70
Ta	0.66	0.28	0.57	1.62	0.29	0.47	0.44	1.26	0.53
Tb	0.33	0.26	0.56	0.22	0.41	0.41	0.33	0.20	0.15
Th	0.54	0.28	0.43	0.18	0.11	0.23	0.17	1.23	0.38
Tl	0.27	0.06	0.17	0.03	0.02	0.02	0.02	0.14	0.44
Tm	0.08	0.07	0.14	0.06	0.11	0.11	0.09	0.06	0.04
U	0.12	0.07	0.11	0.06	0.03	0.07	0.05	0.54	0.09
V	74.40	>370	342.40	>370	>370	>370	>370	>370	360.70
W	3.66	0.05	0.20	0.18	<0.05	0.09	0.06	0.38	0.71
Y	7.01	5.92	12.16	4.94	9.73	9.45	7.62	5.17	3.44
Yb	0.43	0.38	0.75	0.34	0.66	0.63	0.51	0.41	0.23
Zn	139.00	76.00	98.00	319.00	102.00	131.00	125.00	206.00	276.00
Zr	45.00	33.00	50.00	70.00	40.00	41.00	33.00	60.00	33.00

Drill Hole	CL-07-01	CL-07-02	CL-07-03	CL-07-05	CL-07-05	CL-07-05	CL-07-05	CL-07-05	CL-07-05
Depth (m)	422.9	347	169	11	14	30.2	50	105	117
SiO_2(wt%)	38.25	45.37	44.18	15.34	39.97	40.09	39.34	45.27	30.45
TiO_2	4.77	1.47	1.79	>8.00	4.32	4.21	3.53	3.41	4.26
Al_2O_3	16.48	14.99	14.91	4.83	6.46	12.99	9.10	14.21	4.72
Fe_2O_3	22.49	12.80	11.68	50.88	19.85	18.40	19.89	15.11	32.08
MnO	0.20	0.14	0.14	0.36	0.26	0.18	0.18	0.22	0.24
MgO	4.46	8.15	8.34	13.47	11.13	7.96	9.21	5.33	18.08
CaO	6.97	11.68	13.01	0.58	15.00	9.67	13.92	10.72	3.28
Na_2O	2.88	2.31	1.73	0.05	0.63	1.77	0.72	2.87	0.31
K_2O	0.52	0.44	1.12	0.03	0.44	1.26	0.90	1.36	0.32
P_2O_5	0.16	0.01	0.01	0.01	0.04	0.04	0.02	0.17	0.01
L.O.I.	1.28	1.82	2.33	3.18	1.20	2.49	1.81	1.28	5.15
Total	98.46	99.18	99.23	97.09	99.30	99.06	98.63	99.94	98.91
Ba (ppm)	228.50	96.90	888.70	8.30	76.70	278.10	119.30	464.50	52.90
Be	0.73	0.34	0.60	0.08	0.76	0.72	0.40	0.76	1.23
Bi	<0.15	<0.15	<0.15	<0.15	0.17	<0.15	0.29	<0.15	0.17
Cd	0.17	0.12	0.35	0.06	0.39	0.24	0.38	0.14	0.07
Ce	21.86	4.85	5.63	1.41	19.92	8.94	10.65	27.01	44.04
Co	101.95	69.43	53.11	>187	90.62	72.84	109.73	40.72	166.57
Cr	227.00	420.00	547.00	>4500	104.00	9.00	449.00	13.00	2949.00
Cs	1.31	1.23	3.59	0.22	0.58	2.14	2.23	1.28	1.97
Cu	120.40	150.70	100.60	696.10	352.40	112.40	1005.70	10.60	317.50
Dy	1.49	0.90	1.41	0.29	3.53	1.50	1.97	2.84	3.25
Er	0.60	0.42	0.59	0.12	1.47	0.61	0.81	1.13	1.55
Eu	1.46	0.60	0.72	0.11	1.33	0.88	0.94	2.12	0.67
Ga	27.48	19.85	21.55	39.75	19.73	23.43	19.46	22.58	20.00
Gd	2.25	1.10	1.74	0.36	4.43	1.99	2.63	4.03	4.08
Hf	1.25	0.48	0.74	0.59	2.45	1.07	1.58	2.07	6.03
Ho	0.25	0.16	0.24	0.05	0.59	0.25	0.34	0.47	0.58
In	0.06	0.04	0.06	0.08	0.10	0.07	0.10	0.08	0.08
La	9.99	2.29	1.94	0.58	7.38	3.48	3.83	11.30	18.72
Li	28.50	33.90	45.90	10.30	27.10	50.70	40.10	27.80	16.50
Lu	0.06	0.04	0.06	0.01	0.13	0.06	0.08	0.11	0.16
Mo	0.94	0.33	0.35	0.56	0.60	0.47	0.59	1.22	0.67
Nb	8.40	1.21	0.41	3.55	9.63	4.28	4.19	13.30	21.98
Nd	12.80	3.73	5.42	1.16	15.62	7.23	9.02	18.62	23.45
Ni	107.30	205.40	321.20	1318.00	417.20	101.20	852.50	22.80	1011.70
Pb	1.60	5.60	32.40	2.70	5.10	3.40	5.70	5.00	2.10
Pr	2.95	0.75	1.02	0.23	3.13	1.40	1.76	3.94	5.83
Rb	12.32	18.12	38.06	1.07	13.80	33.98	26.25	34.19	24.09
Sb	<0.04	0.07	<0.04	<0.04	<0.04	<0.04	0.07	<0.04	<0.04
Sc	12.20	27.40	30.40	14.60	50.80	32.80	45.10	23.60	14.90
Sm	2.56	1.04	1.64	0.35	4.34	1.95	2.59	4.32	4.91
Sn	0.54	0.45	5.28	0.40	1.10	0.60	3.02	0.76	1.47
Sr	765.60	412.90	467.00	27.40	124.60	458.40	178.20	687.30	96.60
Ta	0.62	0.09	0.04	0.29	0.67	0.32	0.32	0.89	1.33
Tb	0.28	0.16	0.25	0.05	0.64	0.27	0.37	0.53	0.58
Th	0.67	0.10	0.03	<0.018	0.73	0.24	0.42	0.85	3.26
Tl	0.05	0.13	0.27	0.09	0.11	0.15	0.23	0.17	0.24
Tm	0.07	0.05	0.08	0.02	0.18	0.07	0.10	0.14	0.20
U	0.16	0.05	0.02	<0.011	0.23	0.05	0.19	0.26	1.10
V	>370	>370	>370	>370	>370	>370	>370	249.70	>370
W	0.88	0.17	0.85	<0.05	0.28	0.10	0.46	0.88	0.30
Y	6.47	4.31	6.22	1.27	15.24	6.47	8.55	12.20	15.66
Yb	0.42	0.30	0.44	0.10	0.98	0.43	0.58	0.81	1.19
Zn	181.00	117.00	148.00	329.00	120.00	129.00	112.00	113.00	175.00
Zr	43.00	14.00	15.00	17.00	74.00	30.00	43.00	76.00	237.00

Drill Hole	CL-07-05	CL-07-05	CL-07-05	CL-07-05	CL-07-07	CL-07-07	CL-07-07	CL-07-07	CL-07-14
Depth (m)	142.8	144	499	675	10.1	17	450	483	323.5
SiO_2 (wt%)	33.81	38.13	40.18	2.89	44.63	40.62	43.77	46.33	33.43
TiO_2	3.79	2.63	4.43	>8.00	3.54	3.97	4.00	2.58	6.55
Al_2O_3	7.09	10.56	11.86	4.94	13.22	12.21	17.02	10.63	8.75
Fe_2O_3	27.42	21.58	19.22	68.75	16.03	19.70	13.48	13.24	28.51
MnO	0.23	0.19	0.28	0.33	0.19	0.19	0.17	0.20	0.22
MgO	14.44	13.06	5.53	5.00	6.42	7.29	4.79	8.40	8.12
CaO	8.09	7.49	10.95	0.07	11.32	12.03	10.60	15.79	12.18
Na_2O	0.35	0.69	2.26	<0.02	2.45	1.94	3.10	1.85	0.96
K_2O	0.27	1.15	1.32	0.06	0.55	0.54	0.99	0.59	0.20
P_2O_5	0.02	0.04	0.85	0.01	0.08	0.11	0.09	0.07	0.04
L.O.I.	3.25	3.21	1.26	0.04	1.06	0.68	1.18	0.87	0.32
Total	98.76	98.73	98.14	99.11	99.49	99.27	99.19	100.55	99.27
Ba (ppm)	53.80	162.70	503.10	3.60	162.40	145.90	350.40	179.00	67.30
Be	0.22	0.40	17.54	0.10	0.70	0.65	2.39	0.53	0.29
Bi	0.25	0.33	0.37	<0.15	<0.15	<0.15	<0.15	<0.15	<0.15
Cd	0.25	0.28	0.55	0.03	0.15	0.19	0.15	0.17	0.25
Ce	5.44	8.32	270.96	0.74	21.31	21.59	14.63	18.06	9.37
Co	141.21	117.26	71.69	>187	65.21	82.24	53.52	44.16	114.19
Cr	1614.00	1084.00	29.00	176.00	21.00	53.00	20.00	56.00	92.00
Cs	2.16	4.13	4.90	0.03	0.83	0.73	1.47	0.55	0.39
Cu	773.10	900.30	113.30	10.50	84.80	190.30	21.10	20.20	380.40
Dy	1.04	1.14	27.94	0.06	2.99	2.67	1.58	2.82	1.76
Er	0.42	0.49	13.73	0.03	1.26	1.10	0.66	1.11	0.72
Eu	0.50	0.61	4.79	0.07	1.59	1.36	1.20	1.51	0.91
Ga	19.76	19.91	23.42	49.10	21.64	23.69	22.35	16.97	25.06
Gd	1.35	1.48	31.87	0.07	4.03	3.56	2.14	3.94	2.34
Hf	0.90	1.01	25.21	0.86	1.87	2.27	1.01	1.64	1.49
Ho	0.18	0.20	5.17	0.01	0.52	0.45	0.27	0.48	0.30
In	0.07	0.06	0.19	0.09	0.08	0.09	0.05	0.09	0.09
La	2.04	3.48	109.24	0.33	8.16	8.85	6.81	6.64	3.44
Li	60.90	68.60	25.70	1.20	20.70	15.90	26.30	21.90	20.50
Lu	0.04	0.05	1.33	0.00	0.12	0.10	0.06	0.11	0.07
Mo	0.36	0.37	1.66	0.54	0.82	0.83	0.64	1.04	0.74
Nb	2.95	3.58	88.51	7.74	9.52	11.53	7.56	5.48	6.09
Nd	4.59	5.69	146.67	0.39	16.33	14.72	9.56	14.98	8.22
Ni	850.00	790.00	77.00	298.10	94.00	187.40	13.90	47.70	299.40
Pb	2.30	2.90	88.80	0.70	3.10	3.80	6.70	5.50	2.70
Pr	0.88	1.23	35.93	0.10	3.32	3.15	2.04	2.93	1.57
Rb	9.49	30.65	79.16	0.65	17.63	18.68	53.78	20.21	6.04
Sb	<0.04	<0.04	0.08	<0.04	<0.04	<0.04	0.05	<0.04	<0.04
Sc	28.70	24.70	22.30	10.70	24.20	28.70	17.70	39.20	34.10
Sm	1.30	1.51	34.58	0.09	4.16	3.67	2.29	3.97	2.30
Sn	0.88	1.22	>14	1.21	0.95	1.09	3.19	0.64	0.79
Sr	91.30	178.40	478.20	4.90	600.80	527.20	814.30	433.20	306.60
Ta	0.22	0.26	5.89	0.66	0.69	0.75	0.47	0.36	0.44
Tb	0.18	0.20	4.87	0.01	0.55	0.49	0.29	0.54	0.32
Th	0.18	0.55	26.73	0.02	0.59	0.61	0.65	0.48	0.20
Tl	0.19	0.31	0.37	0.03	0.15	0.10	0.24	0.09	0.04
Tm	0.05	0.06	1.80	0.00	0.15	0.13	0.08	0.13	0.08
U	0.04	0.20	3.65	<0.011	0.27	0.20	0.32	0.13	0.05
V	>370	>370	>370	>370	>370	>370	>370	316.40	>370
W	0.16	1.04	3.24	0.20	0.36	0.35	1.01	1.15	0.07
Y	4.46	5.11	135.27	0.27	13.23	11.53	7.44	11.92	7.47
Yb	0.30	0.37	10.37	0.03	0.91	0.77	0.45	0.77	0.50
Zn	178.00	125.00	407.00	396.00	77.00	133.00	106.00	85.00	167.00
Zr	24.00	30.00	1109.00	27.00	58.00	77.00	32.00	48.00	41.00

Drill Hole	CL-07-14	CL-07-15
Depth (m)	477.5	145
SiO_2 (wt%)	40.32	48.62
TiO_2	3.12	1.60
Al_2O_3	13.79	20.77
Fe_2O_3	19.28	9.27
MnO	0.15	0.13
MgO	6.25	1.67
CaO	11.33	8.97
Na_2O	2.15	4.20
K_2O	0.82	1.65
P_2O_5	0.07	0.42
L.O.I.	1.35	2.03
Total	98.64	99.34
Ba (ppm)	278.70	661.30
Be	0.47	0.99
Bi	0.35	<0.15
Cd	0.50	0.13
Ce	15.73	35.53
Co	108.27	23.79
Cr	122.00	20.00
Cs	1.58	1.90
Cu	1226.70	5.10
Dy	2.21	2.18
Er	0.91	0.85
Eu	1.29	2.85
Ga	23.44	25.07
Gd	3.00	3.54
Hf	1.55	1.45
Ho	0.38	0.36
In	0.09	0.08
La	6.18	15.65
Li	23.70	26.70
Lu	0.09	0.08
Mo	1.83	1.72
Nb	6.29	11.03
Nd	11.85	20.76
Ni	906.50	7.20
Pb	9.10	4.30
Pr	2.44	4.78
Rb	25.55	55.18
Sb	0.04	0.05
Sc	25.70	6.00
Sm	3.07	4.22
Sn	2.26	6.85
Sr	558.10	1321.70
Ta	0.44	0.67
Tb	0.41	0.43
Th	0.35	1.00
Tl	0.27	0.28
Tm	0.11	0.10
U	0.12	0.24
V	>370	50.70
W	2.44	1.48
Y	9.54	9.47
Yb	0.62	0.56
Zn	136.00	80.00
Zr	48.00	57.00